Title:

Brain composition in *Heliconius* butterflies, post-eclosion growth and experience-dependent neuropil plasticity

Authors:

Stephen H. Montgomery[1], Richard M. Merrill[2,3], Swidbert R. Ott[4]

Institutional affiliations:

[1] Dept. Genetics, Evolution & Environment, University College London, Gower Street, London, UK, WC1E 6BT

[2] Dept. Zoology, University of Cambridge, Downing Street, Cambridge, UK, CB2 3EJ

[3] Smithsonian Tropical Research Institute, MRC 0580-12, Unit 9100 Box 0948, DPO AA 34002-9998, Panama

[4] Dept. Neuroscience, Psychology and Behaviour, University of Leicester, Adrian Building, University Road, Leicester, UK, LE1 7RH

Corresponding author: Stephen H. Montgomery: Stephen.Montgomery@cantab.net

Associate Editor: Ian A. Meinertzhagen, Dalhousie University

Running head: *Anatomy and plasticity of* Heliconius *brains*

Key words: adaptive brain evolution, comparative neuroanatomy, *Heliconius*, Lepidoptera, mushroom bodies, plasticity

Financial support: This research was supported by research fellowships from the Royal Commission for the Exhibition of 1851 and Leverhulme Trust, a Royal Society Research Grant (RG110466) and a British Ecological Society Early Career Project Grant awarded to SHM. RMM was supported by a Junior Research Fellowship from King's College, Cambridge and an Ernst Mayr Fellowship from STRI. SRO was supported by a University Research Fellowship from the Royal Society, London (UK) and Research Grant BB/L02389X/1 from the BBSRC (UK).

ABSTRACT

Behavioral and sensory adaptations are often reflected in the differential expansion of brain components. These volumetric differences represent changes in cell number, size and/or connectivity, which may denote changes in the functional and evolutionary relationships between different brain regions, and between brain composition and behavioral ecology. Here, we describe the brain composition of two species of *Heliconius* butterflies, a long-standing study system for investigating ecological adaptation and speciation. We confirm a previous report of a striking volumetric expansion of the mushroom body, and explore patterns of differential post-eclosion and experience-dependent plasticity between different brain regions. This analysis uncovers age- and experience-dependent post-eclosion mushroom body growth comparable to that in foraging Hymenoptera, but also identifies plasticity in several other neuropils. An interspecific analysis indicates that *Heliconius* display a remarkably large investment in mushroom bodies for a lepidopteran, and indeed rank highly compared to other insects. Our analyses lay the foundation for future comparative and experimental analyses that will establish *Heliconius* as a valuable case study in evolutionary neurobiology.

INTRODUCTION

Behavioral adaptations typically entail changes in brain function, even if they arise in conjunction with changes in body form or size, or in the number of sensory neurons. In some cases these changes in brain function are reflected in the differential expansion of particular brain regions that betray underlying changes in neuron number or circuitry (Striedter, 2005). Although volumetric differences do not divulge the nature of these underlying structural changes, they can inform the search for the neural substrates of adaptive behavior, particularly in clades with known ecological specializations. The Neotropical genus *Heliconius* (Heliconiinae, Nymphalidae) display a number of striking behavioral adaptations including a dietary adaptation unique among Lepidoptera; adult pollen feeding (Gilbert, 1972, 1975). With the exception of four species formerly ascribed to the genus *Neruda* (Beltrán et al., 2007; Kozak et al., 2015), all *Heliconius* actively collect and ingest pollen as adults. This provides a source of amino acids and permits a greatly extended lifespan of up to six months without reproductive senescence (Gilbert, 1972; Benson, 1972; Ehrlich and Gilbert, 1973). Without access to pollen *Heliconius* suffer a major reduction in longevity and reproductive success (Gilbert, 1972; Dunlap-Pianka et al., 1977; O'Brien et al., 2003).

Several lines of evidence suggest selection for pollen feeding has shaped *Heliconius* foraging behavior. Pollen is collected from a restricted range of mostly cucurbitaceous plants (Estrada and Jiggins, 2002), which occur at low densities (Gilbert, 1975). Individuals inhabit home ranges of typically less than 1 km^2, within which they repeatedly utilize a small number of roosting sites that they return to with high fidelity (Turner, 1971; Benson, 1972; Gilbert, 1975; Mallet, 1986; Murawski and Gilbert, 1986; Finkbeiner, 2014). On leaving the roost, individuals visit feeding sites with a level of consistency in time and space that strongly suggests 'trap-lining' behavior (Ehrlich and Gilbert, 1973; Gilbert, 1975, 1993; Mallet, 1986), analogous to the foraging behavior observed in some species of Neotropical Euglossine bees and bumble bees (Janzen, 1971; Heinrich, 1979). Roosts themselves are located visually (Jones, 1930; Gilbert, 1972; Ehrlich and Gilbert, 1973; Mallet, 1986), and older individuals tend to be more efficient foragers (Boggs et al., 1981; Gilbert, 1993). Together these observations suggest the evolution of pollen feeding in *Heliconius* was facilitated by an enhanced capacity for visually-orientated spatial memory that utilizes

distant landmarks (Gilbert, 1975). The evolution of this behavior likely involves "some elaboration of the nervous system" (Turner, 1981). This elaboration has been suggested to be found in the mushroom bodies, which Sivinski (1989) reported are 3–4× larger in *Heliconius charithonia* than in six other species of butterfly, including two non-pollen feeding Heliconiini, none of which are trap line foragers.

Insect mushroom bodies have a variety of roles in olfactory associative learning, sensory integration, filtering and attention (Zars, 2000; Farris, 2005, 2013; Menzel, 2014). Direct experimental evidence suggests that mushroom bodies mediate place memory in *Periplaneta americana* (Mizunami et al., 1998; Lent et al., 2007), and comparisons across species further suggest that evolutionary expansion of the mushroom body (MB) may be associated with foraging behaviors that depend on spatial memory (Farris, 2005, 2013). For example, phylogenetic comparisons across Hymenoptera demonstrate that the expansion and elaboration of the Euhymenopteran MB coincided with the origin of parasitoidism (Farris and Schulmeister, 2011), a behavioral adaptation that involves place-centered foraging and spatial memory for host location (Rosenheim, 1987; van Nouhuys and Kaartinen, 2008). It is clear, however, that not all evolutionary changes in MB size are linked to place memory. In beetles, phylogenetic expansion and elaboration of the MB has been linked to the evolution of generalist feeding ecologies (Farris and Roberts, 2005). Here, the suggested explanation invokes the 'complexity' of sensory information utilized in foraging, which is thought to be higher in generalist feeders than in specialists, although information content has not been formally quantified.

Ontogenetic plasticity in MB size has likewise been linked to foraging behavior and, possibly, an increased requirement for allocentric memory in this context, particularly in studies on Hymenoptera. Honeybees show two forms of post-eclosion growth in MB volume; age-dependent growth, which occurs regardless of environmental variation, and growth that depends on foraging or social experience (Withers et al., 1993; Durst et al., 1994; Fahrbach et al., 1998, 2003; Capaldi et al., 1999; Farris et al., 2001; Maleszka et al., 2009). In carpenter ants, *Camponotus floridanus*, both nursing and foraging experience contribute to total MB neuropil growth, but foragers exceed nurses in MB size (Gronenberg et al., 1996). Solitary bees (*Osmia lignaria*) with field-foraging experience develop larger MB neuropils than age-matched caged controls (Withers et al., 2008). In paper wasps (*Polybia aequatorialis*), progression through tasks is accompanied by differential growth and

pruning of MB Kenyon cell dendrites, with foragers showing the most extensive branching (Jones et al., 2009). In all these examples, foraging entails spatial orientation and memory as well as the processing of a host of other sensory stimuli not encountered by nurses or caged controls. Sensory stimulation as such contributes to the volumetric increases (in *Bombus impatiens*; Jones et al., 2013), and it therefore remains unclear to what extent the larger MB supports spatial navigation. A less ambiguous link between MB size and spatial navigation can be drawn in desert ants: *Cataglyphis bicolor* have small eyes and optic lobes, but in the MB, the scaling of the visual ('collar') vs. olfactory ('lip') input region resembles that of visually-guided hunting ants, due to a disproportionately large collar volume. In addition, with the onset of foraging, the MB increases in size, particularly in the collar, to far exceed that in age-matched dark-reared individuals (Kühn-Bühlmann and Wehner, 2006). As *Cataglyphis* evidently use their low-resolution vision entirely for spatial navigation (Kühn-Bühlmann and Wehner, 2006), with olfaction dominating the detection of food (Wolf and Wehner, 2000), the evolutionary and foraging experience-related enlargements of their MB collar volume is strongly linked to spatial navigation.

Here we confirm Sivinksi's (1989) observation of a phylogenetic expansion of the MB in *Heliconius*. We further demonstrate age- and experience-dependent plasticity comparable in extent to that reported in Hymenoptera. Together these findings suggest that phylogenetic and ontogenetic changes in MB size reflect an important role in spatial memory, and lay the groundwork for comparative analyses across Heliconiini examining the evolutionary origin and functional importance of MB expansion.

MATERIALS & METHODS

Animals

We collected five males and five females of two species of *Heliconius*, *H. hecale melicerta* and *H. erato demophoon* from wild populations around Gamboa (9°7.4′ N, 79°42.2′ W, elevation 60 m) and the nearby Soberanía National Park, República de Panamá. We assume all wild-caught individuals were sexually mature, and that the age range is not biased between species or sexes. Wild individuals were compared to individuals from first or second-generation insectary-reared stock populations, descended from wild caught parents from the same sampling localities. Stock

populations were kept in controlled conditions in cages (c. 1 × 2 × 2 m) of mixed sex at roughly equal densities. Cages were housed at the *Heliconius* insectaries at the Smithsonian Tropical Research Institute's (STRI) facility in Gamboa. Stocks had access to their preferred host plant (*Passiflora biflora* and *P. vitifolia* respectively for *H. erato* and *H. hecale*), a pollen source (*Psychotria elata*) and feeders containing c. 20% sugar solution with an additional bee-pollen supplement to ensure an excess of pollen. Larvae were allowed to feed naturally on the host plant.

After emergence from the pupae insectary-reared individuals were collected for two age groups, a recently emerged 'young' group (1–3 days post emergence) and an 'old' group (2–3 weeks post emergence). *Heliconius* undergo a "callow" period of general inactivity immediately after emergence that lasts about 5 days, during which flight behavior is weak and males are sexually inactive (Mallet, 1980). These age groups therefore represent behaviorally immature and mature individuals. For *H. hecale* 5 males and 5 females were sampled for both age groups, in *H. erato* 4 males and 6 females were sampled for the 'young' group and 5 males and 4 females were sampled for the 'old' group. In samples for which the exact time of emergence was known there was no significant difference between *H. hecale* and *H. erato* in age structure of the old (*H. erato*: mean = 22.6 days, SD = 8.6; *H. hecale*: mean = 26.4 days, SD = 5.5; t_{13} = -0.899, p = 0.385) or young (*H. erato*: mean = 1.7 days, SD = 0.8; *H. hecale*: mean = 1.3 days, SD = 1.1; t_{17} = 0.829, p = 0.419) insectary-reared groups. Three body size measurements were taken for each individual: body mass, weighted to 0.01 g using a OHAUS pocket balance (model YA102), body length, and wingspan, measured using FreeLOGIX digital calipers. Samples were collected and exported under permits SEX/A-3-12 and SE/A-7-13 obtained from the Autoridad Nacional del Ambiente, República de Panamá in conjunction with STRI.

Antibodies and sera for neuropil staining

We used indirect immunofluorescence staining against synapsin to reveal the neuropil structure of the brain under a confocal microscope (Ott, 2008). This technique exploits the abundant expression of synapsin, a vesicle-associated protein, at presynaptic sites. Monoclonal mouse anti-synapsin antibody 3C11 (anti-SYNORF1; Klagges et al., 1996) was obtained from the Developmental Studies Hybridoma Bank (DSHB), University of Iowa, Department of Biological Sciences, Iowa City, IA

52242, USA (RRID: AB_2315424). The 3C11 antibody was raised against a bacterially expressed fusion protein generated by adding a glutathione S-transferase (GST)-tag to cDNA comprised of most of the 5′ open reading frame 1 of the *Drosophila melanogaster* synapsin gene (*Syn,* CG3985). The binding specificity of this antibody was characterised in *D. melanogaster* (Klagges et al., 1996) and confirmed in synapsin null mutants by Godenschwege et al. (2004). The epitope was later narrowed down to within LFGGMEVCGL in the C domain (Hofbauer et al., 2009). Bioinformatic analysis has confirmed the presence of this motif in lepidopteran genomes, and demonstrated that it is highly conserved across Lepidoptera (Montgomery and Ott, 2015). Binding specificity in *M. sexta* has been confirmed by western blot analysis (Utz et al., 2008) and 3C11 immunostaining has been used as an anatomical marker of synaptic neuropil in a wide range of arthropod species including several Lepidoptera: *D. plexippus* (Heinze and Reppert, 2012), *G. zavaleta* (Montgomery and Ott, 2015), *H. virescens* (Kvello et al., 2009) and *M. sexta* (El Jundi et al., 2009). Cy2-conjugated affinity-purified polyclonal goat anti-mouse IgG (H+L) antibody (Jackson ImmunoResearch Laboratories, West Grove, PA) was obtained from Stratech Scientific Ltd., Newmarket, Suffolk, UK (Jackson ImmunoResearch Cat No. 115-225-146, RRID: AB_2307343).

Immunocytochemistry

Brains were fixed and stained following a published protocol (Ott, 2008). The protocol was divided into two stages, the first of which was performed at the STRI Gamboa Field Station. The brain was exposed under HEPES-buffered saline (HBS; 150 mM NaCl; 5 mM KCl; 5 mM $CaCl_2$; 25 mM sucrose; 10 mM HEPES; pH 7.4) and fixed in situ for 16–20 hours at room temperature (RT) in zinc-formaldehyde solution (ZnFA; 0.25% (18.4 mM) $ZnCl_2$; 0.788% (135 mM) NaCl; 1.2% (35 mM) sucrose; 1% formaldehyde) under agitation. The brain was subsequently dissected out under HBS, washed (3 × in HBS), placed into 80% methanol/20% DMSO for 2 hours under agitation, transferred to 100% methanol and stored at RT. After transportation to the UK samples were stored at -20˚C.

In the second stage of the protocol the samples were brought to RT and rehydrated in a decreasing methanol series (90%, 70%, 50%, 30%, 0% in 0.1 M Tris buffer, pH 7.4, 10 minutes each). Normal goat serum (NGS; New England BioLabs,

Hitchin, Hertfordshire, UK) and antibodies were diluted in 0.1 M phosphate-buffered saline (PBS; pH 7.4) containing 1% DMSO and 0.005% NaN_3 (PBSd). After a pre-incubation in 5% NGS (PBSd-NGS) for 2 hours at RT, antibody 3C11 was applied at a 1:30 dilution in PBSd-NGS for 3.5 days at 4˚C under agitation. The brains were rinsed in PBSd (3 × 2 hours) before applying the Cy2-conjugated anti-mouse antibody 1:100 in PBSd-NGS for 2.5 days at 4˚C under agitation. This was followed by increasing concentrations of glycerol (1%, 2%, 4% for 2 hours each, 8%, 15%, 30%, 50%, 60%, 70% and 80% for 1 hour each) in 0.1 M Tris buffer with DMSO to 1%. The brains were then passed in a drop of 80% glycerol directly into 100% ethanol. After agitation for 30 minutes the ethanol was refreshed (3 × 30 minute incubations), before being underlain with methyl salicylate. The brain was allowed to sink, before the methyl salicylate was refreshed (2 × 30 minute incubations).

Confocal imaging

All imaging was performed on a confocal laser-scanning microscope (Leica TCS SP8, Leica Microsystem, Mannheim, Germany) using a 10× dry objective with a numerical aperture of 0.4 (Leica Material No. 11506511), a mechanical *z*-step of 2 µm and an *x*-*y* resolution of 512 × 512 pixels. Imaging the whole brain required capturing 3×2 tiled stacks in the *x*-*y* dimensions (20% overlap) that were automatically merged in Leica Applications Suite Advanced Fluorescence software. Each brain was scanned from the posterior and anterior side to span the full *z*-dimension of the brain. These image stacks were then merged in Amira 3D analysis software 5.5 (FEI Visualization Sciences Group; custom module 'Advanced Merge'). The *z*-dimension was scaled 1.52× to correct the artifactual shortening associated with the 10× air objective (Heinze and Reppert, 2012; Montgomery and Ott, 2015). Images that illustrate key morphological details were captured separately as single confocal sections with an *x*-*y* resolution of 1024 × 1024 pixels.

Neuropil segmentations and volumetric reconstructions

We assigned image regions to anatomical structures in the Amira 5.5 *labelfield* module by defining outlines based on the brightness of the synapsin immunofluorescence. Within each stack, every forth or fifth image was manually segmented and interpolated in the *z*-dimension across all images that contain the

neuropil of interest. The *measure statistics* module was used to determine volumes (in μm^3) for each neuropil. 3D polygonal surface models of the neuropils were constructed from the smoothed labelfield outlines (*SurfaceGen* module). The color code used for the neuropils in the 3D models is consistent with previous neuroanatomical studies of insect brains (Brandt et al., 2005; Kurylas et al., 2008; El Jundi et al., 2009a, b; Dreyer et al., 2010; Heinze and Reppert, 2012; Montgomery and Ott, 2015).

The whole-brain composite stacks were used to reconstruct and measure six paired neuropils in the optic lobes, and seven paired and two unpaired neuropils in the central brain where distinct margins in staining intensity delineate their margins. All paired neuropils were measured on both sides of the brain in wild-caught individuals to permit tests of asymmetry, yielding two paired measurements per brain (*i.e.* $N = 10 \times 2$) for each structure. We found no evidence of volumetric asymmetry for either species ($p > 0.05$ for each neuropil in paired *t*-tests) and therefore summed the volumes of paired neuropil to calculate the total volume of that structure. In insectary-reared individuals we subsequently measured the volume of paired neuropil from one hemisphere, chosen at random, and multiplied the measured volume by two. We measured the total neuropil volume of the central brain to permit statistical analyses that control for allometric scaling. For the subsequent statistical analyses we analyzed the central body as a single structure and, unless otherwise stated, summed the volumes of the MB lobes and pedunculi.

Intraspecific statistical analyses

In all statistical analyses continuous variables were $\log_{10}$-transformed. Unpaired two-tailed two-sample *t*-tests were used to test for volumetric differences between sexes or groups. We found no evidence of sexual dimorphism in neuropil volume of wild caught individuals that could not be explained by allometric scaling and therefore combined male and female data.

All statistical analyses were performed in R v.3.1 (R Development Core Team, 2008). Our analyses focused on two intra-specific comparisons: i) we compared 'young' and 'old' insectary-reared individuals and interpret significant differences as evidence for post-eclosion growth; and ii) we compared wild-caught individuals with 'old' insectary-reared individuals and interpret significant differences

as evidence for environmentally induced, or experience-dependent plasticity. These comparisons were made by estimating the allometric relationship between each neuropil and a measure of overall brain size (total volume of the central brain minus the combined volume of all segmented neuropil in the central brain: 'rest of central brain', rCBR) using the standard allometric scaling relationship: $\log y = \beta \log x + \alpha$. We used standardized major axis regressions in the SMATR v.3.4-3 (Warton et al., 2012) to test for significant shifts in the allometric slope (β). Where we identified no heterogeneity in β we performed two further tests: 1) for differences in α that suggest discrete 'grade-shifts' in the relationship between two variables, 2) for major axis-shifts along a common slope. Patterns of brain:body allometry were explored in a similar manner, using total neuropil volume as the dependent variable (summed volumes of all optic lobe neuropils plus the total CBR volume), and comparing the results obtained using alternative body size measurements as the independent variable. We also present the effect size, measured by the correlation coefficient (r) calculated from the test statistic from each test of deviation in β, α or major-axis shift . Effect sizes of $0.1<r<0.3$ are interpreted as 'small' effects, $0.3<r<0.5$ 'medium' effects, and $r<0.5$ 'large' effects (Cohen, 1988).

Interspecific statistical analyses

To analyze interspecific patterns of divergence in brain composition we collected published data for neuropil volumes of four other Lepidoptera; *D. plexippus*; (Heinze and Reppert, 2012), *G. zavaleta* (Montgomery and Ott, 2015), *M. sexta*; (El Jundi et al., 2009a) and *H. virescens* (Kvello et al., 2009). Data were available for eight neuropils across all four species. Relative size was measured by calculating the residuals from a phylogenetically-corrected least squares (PGLS) linear regression between each structure and the rest of the brain (total neuropil or CBR as indicated) performed in BayesTraits (freely available from www.evolution.rdg.ac.uk; Pagel, 1999). For this analysis, a phylogeny of the six species was created using data on two loci, *COI* and *EF1a* (GenBank Accession IDs, *COI*: EU069042.1, GU365908.1, JQ569251.1, JN798958.1, JQ539220.1, HM416492.1; *EF1a*: EU069147.1, DQ157894.1, U20135.1, KC893204.1, AY748017.1, AY748000.1). The data were aligned and concatenated using MUSCLE (Edgar, 2004), before constructing a maximum likelihood tree in MEGA v.5 (Tamura et al., 2011). Differences in brain composition across species were analyzed by Principal Component analysis of these

data, and visualized as biplots (Greenacre, 2010) in R package *ggbiplot* (V.Q. Vu, https://github.com/vqv/ggbiplot). Finally, we extended our phylogenetic analysis across insects using a similar approach. We restricted this analysis to volumetric data collected with similar methodology (Rein et al., 2002; Brandt et al., 2005; Kurylas et al., 2008; Dreyer et al., 2010; Ott and Rogers, 2010; Wei et al., 2010). The phylogenetic relationship of these insects was taken from Trautwein et al. (2012).

Nomenclature

We use the nomenclature proposed by the Insect Brain Name Working Group (Ito et al., 2014) with two extensions. We use the term *lobe mass* (LBM) to refer to the tightly fused synapse-dense neuropil mass in *Heliconius* that comprises the homologues of the medial lobe, vertical lobe and Y lobe of the MB (and possibly further satellite neuropils not present or as yet unidentified in Lepidoptera). Heinze and Reppert (2012) recently described a discrete neuropil in the optic lobe of *Danaus plexippus* that had not been described in other Lepidoptera. They introduced the term *optic glomerular complex* (OG) to describe this neuropil. Subsequently, Kinoshita et al. (2014) used 'ventral lobe of the lobula' (vLO) to describe a similar, and potentially homologous, structure in *Papilio xuthus*. We prefer this to Heinze and Reppert's OG, to avoid confusion with the term 'optic glomeruli' (also abbreviated to OG) which is reserved for synapse-dense foci in the ventrolateral neuropils first described in Diptera (Strausfeld and Okamura 2007; Ito et al., 2014). However, we note the vLO may not be derived from the LO but could instead represent an OG that has moved into the optic lobe (see Results). It may therefore be necessary to revisit the nomenclature of this neuropil at a later date. All other abbreviations are defined at first use.

RESULTS

General layout of the *Heliconius* brain

The overall layout and morphology of the *Heliconius* brain (Fig. 1) is similar to that of other Lepidoptera (El Jundi et al., 2009; Kvello et al., 2009; Heinze and Reppert, 2012; Montgomery and Ott, 2015). The central brain (CBR) forms a single medial mass, containing the cerebrum to which the gnathal ganglia are fused. Together with the rest of the CBR (rCBR), which lacked sufficiently clear internal boundaries for

unambiguous further segmentation in our synapsin-stained preparations, we measured the volumes of six paired neuropils in the optic lobes, and eight paired and two unpaired neuropils in the central brain in 59 individuals across both species (Table 1).

Sensory neuropil

The large optic lobes (OL; Fig. 2) account for approximately 64% of the total brain volume. As is the case in both *D. plexippus* and *G. zavaleta,* the lamina (LA), two-layered medulla (ME) (Fig. 2E), accessory medulla (AME), lobula (LO) and lobula plate (LOP) are well defined and positioned in the OL as nested structures from lateral to medial (Fig. 2A). The LA has a distinct, brightly synapsin-immunoflourescent inner rim (iRim; Fig. 2E), a feature common to all diurnal butterflies analyzed thus far (Heinze and Reppert, 2012; Montgomery and Ott, 2015). In common with *D. plexippus* we identify a thin strip of irregularly shaped neuropil running ventrally from the AME to the ME (Fig. 2G–H).

We also identify a sixth neuropil in the OL (Fig. 2B,F) that we believe to be homologous to the 'optic glomerular complex' first identified in *D. plexippus* and postulated to be Monarch-specific by Heinze and Reppert (2012). A similar neuropil has since been described in *Papilio xuthus*, referred to as the 'ventral lobe of the LO' or vLO (Kinoshita et al., 2015). Here we use Kinoshita et al.'s vLO to avoid confusion with the use of 'Optic Glomeruli' as a descriptor for complex of synapse-dense visual foci in the ventrolateral CBR (Ito et al., 2014). In *Heliconius*, as in *D. plexippus*, the vLO is a multi-lobed, irregularly shaped structure positioned to the medial margin of the LOB with which it appears to be connected. In *Heliconius* the vLO is not as extended in the anterior margin as in *D. plexippus* and is subsequently confined to the OL, without protrusion into the optic stalk or cerebrum (Fig. 2A,B,F). The position of the vLO in *Heliconius* is also similar to that of a dramatically smaller neuropil observed in *G. zavaleta* (Montgomery and Ott, 2015) that may be homologous. At a wider phylogenetic scale, the vLO may be homologous with one or a subset of the optic glomeruli in the ventrolateral neuropils of flies and other insects (Ito et al., 2014) that has shifted position into the OL in butterflies.

The CBR contains further optic glomeruli, including the anterior optic tubercle (AOTU). We identify the same four components of the AOTU as previously described in *D. plexippus* and *G. zavaleta* butterflies (Heinze and Reppert, 2012; Montgomery and Ott, 2015): the small, closely clustered nodular unit (NU), strap (SP)

and lower unit (LU), and the much larger upper unit (UU) (Fig. 2C). As in other butterflies, the UU is expanded compared with nocturnal moths (El Jundi et al., 2009; Kvello et al., 2009). The proportion of total neuropil comprised of the AOTU is, however, larger in *D. plexippus* (0.74%) than *Heliconius* (0.40% in *H. hecale* and 0.37% in *H. erato*).

The antennal lobes (AL), the primary olfactory neuropil, are comprised of small, round glomeruli that are innervated by axons from olfactory sensory neurons in the antennae. These glomeruli are arranged around a central fibrous neuropil, the AL hub (ALH) (Figure 3A,B). In *Heliconius* the AL comprises 2% of the total brain neuropil volume, and contains approximately 68 glomeruli (estimated in one individual of each sex: *H. erato* ♂ = 69, ♀ = 68; *H. hecale* ♂ = 68, ♀ = 67) which is similar to the number of olfactory receptor genes (70) identified in the *H. melpomene* genome (Dasmahapatra et al., 2012). We found no expanded macro-glomerular complex (MGC) or obvious candidates for sexually dimorphic glomeruli. This is in keeping with all diurnal butterflies described to date (Rospars, 1983; Heinze and Reppert, 2012; Carlsson et al., 2013), with the exception of the more olfactorily orientated *G. zavaleta* (Montgomery and Ott, 2015).

We took advantage of comparable datasets for *H. erato, H. hecale* and *G. zavaleta* to investigate whether changes in relative AL volume are due to an increased volume of glomeruli or ALH. Both glomerular and ALH volume are larger in *G. zavaleta* relative to the CBR, as indicated by significant grade-shifts in allometric scaling in *G. zavaleta* and *Heliconius* (glomerular, *H. erato*: Wald $\chi2 = 10.709$, $p = 0.001$; *H. hecale*: Wald $\chi2 = 9.139$, $p = 0.003$; ALH, *H. erato*: Wald $\chi2 = 30.282$, $p < 0.001$; *H. hecale*: Wald $\chi2 = 26.638$, $p < 0.001$). However, ALH expansion in *G. zavaleta* is disproportionately large, driving a grade-shift in the scaling relationship between glomerular and ALH volume in *G. zavaleta* when compared with either *Heliconius* (*H. erato*: Wald $\chi2 = 19.680$, $p < 0.001$; *H. hecale*: Wald $\chi2 = 31.663$, $p < 0.001$; Fig. 3D).

Central complex

The central complex (CX) is a multimodal integration center linked to a range of functions from locomotor control to memory (Strauss 2002; Bender et al., 2010; Pfeiffer and Homberg, 2014). Within the limitations of the current analysis, the anatomy of the *Heliconius* CX shows strong conservation with *D. plexippus* and *G.*

435 *zavaleta* (Heinze and Reppert, 2012; Montgomery and Ott, 2015). The central body
436 (CB) is positioned along the midline of the CBR and is formed of two neuropils, the
437 upper (CBU) and lower (CBL) divisions, which are associated with small paired
438 neuropils, the noduli (NO), located ventrally to the CB (Fig. 4A–D,G). Two further
439 paired neuropils, the protocerebral bridge (PB; Fig. 4A,E) and posterior optic
440 tubercles (POTU; Fig. 4A,F), are positioned towards the posterior margin of the brain.
441
442 **Mushroom bodies**
443 The most striking aspect of *Heliconius* brain morphology are the hugely expanded
444 MBs which span the depth of the brain along the anterior-posterior axis (Fig. 5). On
445 the anterior side, the MB lobes lie above the AL. As in *D. plexippus* (Heinze and
446 Reppert, 2012), the distinct boundaries between the medial lobe (ML), vertical lobe
447 (VL) and Y lobe (YL) observed in moths (El Jundi et al., 2009; Kvello et al., 2009)
448 are lost, possibly due to extensive expansion. The only identifiable feature is a lobe
449 curving round the medial margin, likely to be part of VL (Fig. 5D,F). We therefore
450 refer to the entire synapse-dense neuropil mass that corresponds to the ML, VL and
451 YL of moths as the lobe mass (LBM). The LBM merges with the cylindrical
452 pedunculus (PED) that extends to the posterior cerebrum. The boundary between the
453 LBM and PED is not distinct. The combined volume of the PED+LBM accounts for
454 12.2% of total CBR volume in *H. hecale* and 14.6% of total CBR volume in *H. erato*,
455 at least twice that reported for other Lepidoptera (Sjöholm et al., 2005; El Jundi et al.,
456 2009; Kvello et al., 2009; Heinze and Reppert, 2012; Montgomery and Ott, 2015). At
457 the posterior end, the PED splits into two roots that are encircled by the MB calyx
458 (CA; Fig. 5A,H,K). A Y tract (YT) runs parallel to the PED from the posterior
459 boundary of the LBM to the junction between the PED and CA. The YT ventral
460 loblets seen in other Lepidoptera (El Jundi et al., 2009; Kvello et al., 2009) are not
461 distinct, having merged into the LBM (Fig. 5A,J,N).
462 The CA of *Heliconius* has a deeply double-cupped morphology (‘double
463 calyx’ type; Fig. 5A,C). Two concentric zones can be identified (Fig. 5E), though the
464 boundary is not distinct throughout the depth of the neuropil. The CA comprises
465 20.7% and 23.9% of total CBR volume in *H. hecale* and *H. erato* respectively, at least
466 three times greater than reported in other Lepidoptera (Sjöholm et al., 2005; El Jundi
467 et al., 2009; Kvello et al., 2009; Heinze and Reppert, 2012; Montgomery and Ott,
468 2015). In some individuals the CA is so large that it protrudes into the OL, resulting

in a distortion of shape caused by constriction around the optic stalk (Fig. 5H). We also observe some degree of pitting in the posterior surface of the CA (Fig. 5I). This pitting is related to radially arranged columnar domains that are apparent within the calycal neuropil (Fig. 5J,K). We do not observe any structure clearly identifiable as an accessory calyx. We do see a brightly stained globular neuropil below the CA / PED junction but it is quite some distance away from the junction and lacks the 'spotty' appearance of the accessory calyx in *D. plexippus* (Heinze and Reppert, 2012). It seems more likely that this structure is a 'satellite' neuropil that is not part of the MB (Farris, 2005). Its position corresponds roughly to the medial end of the expanded vLO in *D. plexippus*. In some preparations one can follow a narrow faint fiber tract from here to an area of more intense staining in the optic stalk and on to the medial margin of the vLO. If this is a functional connection, it is conceivable that the medial expansion of the vLO in *D. plexippus* occurred along this pre-existing pathway.

Interspecific divergence in brain composition and mushroom body expansion in *Heliconius*

After correcting for allometric scaling using phylogenetically-corrected regressions against total neuropil volume, the six lepidopteran species can be separated along the first two principal components (PC) that together explain 90.7% of variance. PC1 (65.9% of Var) is heavily loaded by sensory neuropil in one direction, and CA and PED+LBM in the other (Table 2). PC2 (24.8% of Var) is heavily loaded by the ME in one direction and the AL and CB in the other. This roughly separates the six species into three pairs, representing (i) *H. hecale* and *H. erato*; (ii) the other diurnal butterflies, *D. plexippus* and *G. zavaleta*; and (iii) the night-flying moths, *H. virescens* and *M. sexta* (Fig. 6B). When CBR neuropils are analyzed separately, PC1 (68.7% of Var) marks an axis dominated by AL, CB and MB, whilst PC2 (23.3% of Var) is strongly loaded by the AOTU (Fig. 6C). This leads to two clusters grouping (i) *H. hecale* and *H. erato*, which invest heavily in MB neuropil, and (ii) the night-flying moths and *G. zavaleta*, which invest heavily in olfactory neuropil; leaving *D. plexippus* isolated by its large relative AOTU volume.

The combined volume of CA, PED and LBM accounts for 13.7% of total brain neuropil volume in *H. erato*, and 11.9% in *H. hecale*. This is much larger than reported for any other Lepidoptera measured with similar methods (range 2.3–5.1%). Expressed as a percentage of the CBR to remove the effects of variation in the OL,

503 which vary greatly in volume between nocturnal and diurnal species, *H. erato*
504 (38.5%) and *H. hecale* (32.9%) again exceed other Lepidoptera (4.8–13.5%) by 3–7
505 fold. These figures are also much larger than reported for *H. charithonia* (4.2% of
506 total brain size) by Sivinski (1989), whose figures for other Lepidoptera are also
507 much lower suggesting the discrepancy is explained by difference in methodology.
508 Beyond Lepidoptera, the most comparable data available are from *Apis*
509 *mellifera* (Brandt et al., 2005) and *Schistocerca gregaria* (Kurylas et al., 2008) for
510 which MB and CBR volumes are reported (Fig. 6D). In terms of raw volume (Table
511 1), *Heliconius* MBs are roughly equal in size to *A. mellifera*. However, in *A. mellifera*
512 the MBs comprise 65.4% of the CBR (40.6% CA, 24.8% PED+LBM) (Brandt et al.,
513 2005), in gregarious-phase *S. gregaria* they comprise 15.1% (8.2% CA including the
514 accessory calyx, 6.3% PED+LBM) (Kurylas et al., 2008). Further comparisons can be
515 made expressing MB size as a percentage of segmented neuropils (ME, LO, LOP,
516 CB, MB and AL) that were labeled across a wider range species. In the ratio of
517 percentage MB volume to the percentage of the two other CBR neuropils (AL and
518 CB), *H. erato* (6.4) and *H. hecale* (6.7) far exceed even *A. mellifera* (3.8). To account
519 of the dominant effect of OL size on scaling with overall brain size, we also analyzed
520 residual variance from a PGLS regression (Fig. 6E) between percentage OL and
521 percentage MB volume. This shows *Heliconius* (*H. erato*: +8.2; *H. hecale*: +7.5) have
522 the second largest residual MB size following *A. mellifera* (+11.9).
523
524 **Brain : body allometry**
525 In wild individuals of both species the brain : body size relationship is significant
526 when using total neuropil volume and either body length or wingspan as measures of
527 brain and body size ($\log_{10}$-$\log_{10}$ SMA regression, *H. hecale,* body length $p = 0.020$;
528 wingspan $p = 0.019$; *H. erato,* body length $p = 0.011$; wingspan $p = 0.010$). The brain
529 size : body mass relationship is not significant in wild individuals (*H. hecale,* $p =$
530 0.055; *H. erato,* $p = 0.863$), most likely because body mass varies much with
531 reproductive state and feeding condition. We therefore used body length as a proxy
532 for body size to analyze the effect of age and experience on the relative size of the
533 brain.
534 Both species showed a clear grade-shift with age towards increased relative
535 brain size (*H. hecale:* Wald $\chi^2 = 5.780$, $p = 0.016$; *H. erato:* Wald $\chi^2 = 10.124$, $p =$
536 0.001). Body length was very similar in old and young individuals (*H. hecale* $t_{18} =$ -

0.918, p = 0.371; *H. erato* t_{17} = 0.581, p = 0.568) suggesting the effect reflects an increase in absolute neuropil volume. Indeed, old individuals had significantly larger absolute CBR volumes in both species (*H. erato:* t_{17} = 4.192, p = 0.001, r = 0.713; *H. hecale:* t_{18} = 3.054, p = 0.007, r = 0.595; Fig. 7A,D). An absolute increase in OL and total brain volume, however, was strongly supported only in *H. erato* (OL: t_{17} = 5.076, p < 0.001, r = 0.776; total, t_{17} = 5.153, p < 0.001, r = 0.708) and not evident in *H. hecale* (OL, t_{18} = 0.280, p = 0.783; total, t_{18} = 1.082, p = 0.293).

Only *H. hecale* showed a clear response in overall brain size to experience. The total neuropil was 40% larger in wild-caught than in old insectary-reared individuals (t_{17} = 2.553, p = 0.020, r = 0.526) driven by a significant difference in CBR volume (t_{17} = 3.658, p = 0.002, r = 0.664), but not OL volume (t_{18} = 1.728, p = 0.101; Fig. 7D). Although there was no matching difference in body length (t_{18} = 0.983, p = 0.436), a grade-shift towards larger relative brain size in wild *hecale* was not supported (Wald χ^2 = 2.058, p = 0.151). However, we do observe a grade-shift when the CBR is analyzed separately (Wald χ^2 = 4.725, p = 0.030). No significant brain or body size differences were found between wild and old insectary-reared individuals in *H. erato* (total neuropil: t_{17} = -0.432, p = 0.671; CBR: t_{17} = -0.732, p = 0.474; OL: t_{17} = -0.123, p = 0.904; body length: t_{17} = 1.009, p = 0.327; Fig. 7A).

Post-eclosion growth in the volume of individual neuropil regions

The age-related increase in overall absolute brain size in *H. erato* was reflected in volumetric increases in nearly all brain regions, with only the vLO failing to show a significant expansion in old individuals (Table 3A). There was some evidence for age-related differences in the allometric scaling coefficients for AME and PB, and for grade-shifts in vLO and POTU, but these were weak relative to the strong major axis shifts observed for all neuropils investigated (Table 3A). The largest shifts were observed for the POTU (difference in fitted-axis mean, Δ_{FA} = 0.604), AME (Δ_{FA} = 0.536), CA (Δ_{FA} = 0.496) and PED+LBM (Δ_{FA} = 0.393; Fig. 8A-C).

In contrast, in *H. hecale,* age-related size increases in volume were confined to the CBR and not all segmented regions within it showed the same pattern of expansion; the rCBR, components of the MB, CX and AL were all significantly larger in old individuals, but the AOTU, POTU and all OL neuropil were not (Table 3B). Neuropil expansion appears to occur in a coordinated manner, such that the allometric relationship between each neuropil and rCBR is maintained (Table 3B). The only

exceptions were the LA, ME and vLO, which showed significant grade-shifts towards a reduced volume relative to rCBR in old individuals. All other segmented neuropils showed major-axis shifts along a common slope towards higher values in old individuals (Table 3B). The largest shifts were observed in the MB (CA, $\Delta_{FA} = 0.279$; PED+LBM, $\Delta_{FA} = 0.250$; Fig. 8A1–C1).

Experience-dependent plasticity in neuropil volume

Although wild *H. erato* do not have significantly larger absolute volumes for any measured neuropil (Table 4A), differences in allometric scaling or grade-shifts between wild and old insectary-reared individuals are nevertheless evident. Altered scaling affects the AME, CA, LOP, CBL+CBU and PB, all of which show shallower scaling relationships (smaller β) with rCBR in wild-caught individuals (Table 4A; Figure 7B,C). The PED+LBM shows both an unambiguous grade-shift towards larger size in wild whilst maintaining a common slope, and a major axis shift ($\Delta_{FA} = 0.250$; Fig. 8B1).

In *H. hecale* wild individuals have a significantly larger CBR ($t_{18} = 3.658$, $p = 0.002$). The only segmented neuropil to reflect this difference, however, are the CA and PED+LBM of the MB (Table 4B; Fig. 8A2,C2), while the rCBR is also larger in wild individuals ($t_{18} = 3.417$, $p = 0.003$). The average CA volume of old insectary-reared individuals is only 68.3% of the average wild CA volume, for the young insectary-reared individuals it is 49.3% (Figure 8A2,C2). For PED+LBM these figures are 76.9% and 58.7% respectively (Figure 8A2,B2). For comparison, in *H. erato* the average CA volume of old insectary-reared individuals is 96.2% of the average wild CA volume, for the young insectary-reared individuals it is 59.7% (Fig. 8A1–C1). For PED+LBM these figures are 96.9% and 63.9% respectively (Fig. 8A1–C1).

The only neuropil in the OL to differ significantly in volume in *H. hecale* is the ME. The allometric relationship between neuropil volumes and rCBR differs for all neuropils either in the allometric scaling coefficient or the intercept, except for the MB components and AME (Table 4A; Figure 7E,F). However, for AME this pattern is caused by a lack of allometric scaling in insectary-reared individuals (SMA $p = 0.552$). The MB shows evidence of a major axis shift along a common slope (CA, $\Delta_{FA} = 0.355$; LBM, $\Delta_{FA} = 0.299$; Fig 8B2, C2). Given all grade-shifts result in smaller

neuropil volumes relative to rCBR (Fig. 7E,F) we interpret this as indicating that rCBR and MB show coordinated environment-dependent increases in volume whilst other neuropil volumes remain largely constant, but with subsequently altered allometric relationships with rCBR.

Allometric scaling of mushroom body components

We further explored the allometric scaling relationships between the three main MB components, the LBM and PED (analyzed separately), and the CA. Within wild caught individuals, pairwise comparisons between these structures do not reveal any significant deviation from isometric scaling relationships (test $\beta \neq 1$, $p > 0.05$). However, the ontogenetic growth we observe between the young and old groups of both species occur through concerted expansion of the LBM and CA (i.e. a major axis shift), both of which show grade-shifts in their allometric scaling with the PED between the young and old groups (Table 5A). A similar pattern is found comparing *H. hecale* wild and old groups, but there are no significant differences between wild and old *H. erato* with the exception of a narrowly significant difference in the scaling coefficient suggesting LBM becomes disproportionally larger as CA increases in wild compared to insectary-reared old individuals (Table 5B).

DISCUSSION

We have described the layout and volume of the major brain neuropils in two species of *Heliconius* butterflies. Our interspecific analyses illustrate the role ecology plays in shaping brain structure, and confirm the substantial evolutionary expansion of the *Heliconius* MB first noted by Sivinski (1989). Indeed, our data suggest this previous work underestimated their size. We have further identified neuropil-specific patterns of volumetric variation across young and old insectary-reared and wild individuals that indicate significant age- and experience-dependent growth. In the MB, the timing and extent of this ontogenetic plasticity is comparable to that found in insects that strongly rely on spatial memory for foraging (e.g. Withers et al., 1993, 2008; Gronenberg et al., 1996; Fahrbach et al., 1998, 2003; Maleszka et al., 2009).

Interspecific divergence and mushroom body expansion in Heliconius

Our interspecific analyses across Lepidoptera reveal an unambiguously mosaic pattern of brain evolution (Barton and Harvey, 2000), where the size of individual neuropils deviate from the allometric expectation. Mosaic patterns in mammals, fishes and ants have been interpreted as strong evidence for evolutionary responses to a species' particular ecological needs (Barton et al., 1995; Huber et al., 1997; Gronenberg and Hölldobler, 1999). Across Lepidoptera, this is particularly noticeable in the sensory neuropils (Fig. 6B). The relative volume of the visual neuropils closely reflects diel activity patterns, and the size of the AL also appears to be strongly associated with a nocturnal or low-light diurnal niche. This is illustrated in a PCA of central brain neuropil (Fig. 6C) that clusters the olfactorily driven butterfly *G. zavaleta* with night-flying moths (Montgomery and Ott, 2015). Our interspecific comparisons further indicate that much of the divergence in AL size among Lepidoptera reflects changes in ALH volume rather than total glomerular volume (Figure 3C,D), implying that changes in the number or branching complexity of AL projection neurons and/or local interneurons dominate over numerical differences in olfactory sensory neuron supply, and associated sensitivity. Furthermore, the relative constancy in AL glomeruli number indicates that the dimensionality of the afferent coding space is comparable across species of Lepidoptera with divergent diel patterns (Boeckh and Boeckh, 1979; Rospars, 1983; Berg et al., 2002; Huetteroth and Schachtner, 2005; Masante-Roca et al., 2005; Skiri et al., 2005; Kazawa et al., 2009; Heinze and Reppert, 2012; Carlsson et al., 2013; Montgomery and Ott, 2015).

In contrast with other species differences that are dominated by changes in the sensory neuropils, amongst Lepidoptera *Heliconius* are clearly set apart in our multivariate analysis along an axis heavily loaded by the MB. As a percentage of total brain volume, or indeed as a raw volume, *Heliconius* have the largest MB so far reported in Lepidoptera (Sivinski, 1989; Sjöholm et al., 2005; Rø et al., 2007; Kvello et al., 2009; Snell-Rood et al., 2009; Dreyer et al., 2010; Heinze and Reppert, 2012; Montgomery and Ott, 2015) and one of the largest across insects. This phylogenetic expansion of the *Heliconius* MB is likely to reflect an adaptive response to ecological selection pressures that arise from the derived pollen-feeding behavior (Sivinski, 1989). Several studies have reported this behavior to entail spatially and temporally faithful foraging patterns, guided by visual landmarks (Ehrlich and Gilbert, 1973; Gilbert, 1975, 1993; Mallet, 1986) comparable with the landmark-based trap-lining foraging behavior of some species of Neotropical Euglossine bees and bumble bees

(Janzen, 1971; Heinrich, 1979). Experimental interventions (Mizunami et al., 1998) and comparative neuro-ecological studies (Farris and Schulmeister, 2011) likewise implicate MBs in visually based spatial memory.

Comparisons across *Heliconius* and non-pollen feeding Heliconiini may provide a test of this spatial memory hypothesis. Sivinski (1989) reported that two individuals of *Dione juno* and *Dryas iulia*, both non-pollen feeding allies to *Heliconius*, had MBs within the size range of other Lepidoptera. This provides preliminary support that MB expansion coincided with a single origin of pollen feeding at the base of *Heliconius*. However, sampling in a wider range of genera, including the specious *Eueides* which is most closely related to *Heliconius* (Beltrán et al., 2007; Kozak et al., 2015), is required to confirm this conclusion.

Alternative selection pressures also need to be considered, including the degree of host-plant specialization (Brown, 1981) and the evolution of social roosting (Benson, 1972; Mallet, 1986). These factors may well be inter-related, as visits to *Passiflora* may be incorporated into trap-lines between pollen plants (Gilbert, 1975, 1993), and the sedentary home-range behavior required for trap-lining may predispose *Heliconius* to sociality (Mallet, 1986). The latter scenario would parallel the hypothesized origin of sociality in Hymenoptera and primates in exaptations of an expanded brain that may have first evolved to support specialization in foraging behavior (Barton, 1998; Farris and Schulmeister, 2011). Regardless of whether pollen feeding provided the initial selection pressure for MB expansion in *Heliconius*, it is likely that it contributes to meeting the energetic cost of this increased neural investment.

Age- and experience-dependent growth in neuropil volume

In both *H. erato* and *H. hecale*, the MBs are significantly larger in aged individuals. Volume increases of 38.0% for the CA and 34.0% for the LBM in *H. erato,* and 27.9% for the CA and 23.7% for the LBM in *H. hecale* are comparable to, if not greater than, the ontogenetic changes seen in Hymenoptera (e.g. c. 30% in *Camponotus floridanus* (Gronenberg et al., 1996); c. 20% in *Bombus impatiens* (Jones et al., 2013)). Our comparisons between aged insectary-reared and wild-caught individuals also identify experience-dependent plasticity. This ‘experience’ in the wild likely includes greater range of movement, greater challenges in foraging, and more variable environmental conditions and social interactions.

Our data suggest experience-dependent plasticity particularly affects MB maturation, though the pattern differs between species. In *H. hecale* a strong volumetric difference is found between old insectary-reared and wild caught individuals for both the CA (32%) and LBM (24%). A concomitant expansion of the rCBR results in a pronounced major-axis shift. This is not simply the result of an increased total brain size, however: no other neuropil region shows a comparable increase in wild caught individuals, resulting in widespread grade-shifts in these other neuropils towards smaller size relative to the rCBR. This may reflect a coordinated growth between the MB and specific brain regions within the rCBR or, alternatively, coincident independent expansions. In *H. erato,* old insectary-reared and wild-caught individuals have MBs of similar absolute size, but allometric grade-shifts over the rCBR result in greater relative volumes in wild compared to insectary-reared individuals. The cause of this species difference is unclear, but warrants further investigation.

Finally, it is also notable that plasticity, and particularly age-related growth, is not restricted to the MB. Several visual and olfactory neuropils show age- and experience-dependent expansions in *Heliconius,* as they do in other insects (Kühn-Bühlmann and Wehner, 2006; Snell-Rood et al., 2009; Ott and Rogers, 2010; Smith et al., 2010; Heinze and Florman, 2013; Jones et al., 2013). We also find evidence of plasticity in components of the CX. In *D. plexippus*, size plasticity in the CX and PB has been proposed to be linked to migratory experience (an inferred long-distance migration of >500km) and, by association, the sky compass navigation that supports it (Heinze et al., 2013). Our results in *Heliconius* show that similar ontogenetic increases in CX size coincide with foraging that entails land-mark based navigation at much smaller spatial scales.

Functional relevance of phylogenetic mushroom body expansion

Phylogenetic trends towards larger MBs involve increases in Kenyon cell (KC) numbers, clustered into larger numbers of functional sub-units (Farris, 2008). Farris and Roberts (2005) suggest that increasing KC number may provide greater computational capacity by facilitating the processing of more complex combinatorial inputs from afferent projection neurons (Sivan and Kopell, 2004), or through integration across increasingly specialized sub-units (Strausfeld, 2002).

Novel pathways between such specialized KC sub-populations may play an important role in the origin of derived behaviors that require the integration of different sensory modalities (Chittka and Niven, 2009; Strausfeld et al., 2009). Examples of this are provided by Hymenoptera and phytophagous scarab beetles where, in addition to olfactory inputs, the MB calyx receives direct input from the optic lobes (Gronenberg, 2001; Farris and Roberts, 2005; Farris and Schulmeister, 2011). This additional input is reflected in the subdivision of the CA into the lip, which processes olfactory information, and the collar and basal ring, which process visual information (Gronenberg and Hölldobler, 1999). Visual input to the MB has also been demonstrated in some butterflies (Snell-Rood et al., 2009; Kinoshita et al., 2015) and moths (Sjöholm et al., 2005), but it has yet to be investigated in *Heliconius*. The *Heliconius* CA lacks the clear zonation observed in *D. plexippus* (Heinze and Reppert, 2012) and *P. xuthus* (Kinoshita et al., 2015) that has been suggested to be analogous to the *A. mellifera* lip, collar and basal ring (Heinze and Reppert, 2012). We do not interpret the lack of distinct zonation in *Heliconius* as evidence against functional sub-division, as *Spodoptera littoralis* displays localization of visual processing in the CA that is not apparent without labeling individual neurons. Given the implied role for visual landmark learning in *Heliconius* foraging behavior (Jones, 1930; Gilbert, 1972, 1975; Mallet, 1986), and the phylogenetic distribution of visual input to the CA in Lepidoptera, we hypothesize that their massively expanded MBs may support integration of visual information.

In other species the MB also receives gustatory and mechanosensory input (Schildberger, 1983; Homberg, 1984; Li and Strausfeld, 1999; Farris, 2008). These may also be of relevance in *Heliconius* given the importance of gustatory and mechanosensory reception in host-plant identification (Schoonhoven, 1968; Renwick and Chew, 1994; Briscoe et al., 2013) and pollen loading (Krenn and Penz, 1998; Penz and Krenn, 2000), although it should be noted that there is currently no evidence these behaviors are learnt (Kerpel and Moreira, 2005; Salcedo, 2011; Silva et al., 2014).

Potential cellular changes associated with ontogenetic mushroom body expansion

The cellular basis of ontogenetic and environmentally induced plasticity may provide further clues to the functional changes associated with MB expansion during *Heliconius* evolution. The volumetric changes we observe in MB size must reflect

differences in cell numbers and/or branching and connectivity. Concerning cell numbers, we know of no precedent for adult neurogenesis of AL projection neurons or of MB extrinsic interneurons that innervate the lobes. Adult neurogenesis of KCs is a distinct possibility, however. While KC neurogenesis is reportedly absent in adult *D. plexippus* (Nordlander and Edwards, 1969), it has evolved independently multiple times and does occur in young adults of the moth *Agrotis ipsilon* (Cayre et al., 1996; Dufour and Gadenne, 2006). It is conceivable that *Heliconius* have evolved extensive adult KC neurogenesis to support their the unusually long lifespan and strong reliance on memory. Adult neurogenesis is not, however, *required* for pronounced changes in MB volume: Hymenoptera lack it (Fahrbach et al., 1995), with post-eclosion volumetric expansion resulting solely from increased neurite branching (Gronenberg et al., 1996; Farris et al., 2001). In Hymenoptera, age-dependent expansion of the CA accompanies growth of extrinsic neuron processes, whilst increased branching of KCs is instead associated with experience-dependent expansion and foraging specialization in social castes (Farris et al., 2001; Jones et al., 2009). Increases in KC connectivity, and associated increases in fiber outgrowth and synaptic spine proliferation, and/or alterations in arborizations in the lobes can be sufficient to explain ontogenetic MB growth.

We found no evidence of deviation from isometric scaling between CA and LBM in wild individuals, which contrasts with the pronounced hyperallometry of CA over lobes reported in *Apis mellifera* (Mares and Ash, 2005) and *Schistocerca gregaria* (Ott and Rogers, 2010). Ott and Rogers (2010) proposed that this hyperallometry reflects a non-linear increase in 'wiring' (the total amount of axons and dendrites; Sterling and Laughlin, 2015) required to connect increasing numbers of KCs with their synaptic partners. Applying this argument to the *Heliconius* MB, the isometric scaling between CA and LBM might indicate that overall size differences do not arise through major differences in KC numbers. The disproportionate expansion of CA and LBM volume over PED volume observed in old individuals of both species, and in wild *H. hecale*, can also be explained without invoking the addition of new cells if many KCs undergo similar changes in total branch volume in CA and LBM that are not matched by proportional changes in PED. We consider this more likely than an alternative explanation reliant on increasing cell number, which would require substantial post-eclosion neurogenesis of KCs that differ profoundly in their average volumetric proportions in the CA, PED and LBM. Experimentally

confirming the relative roles of increased neuritic growth and post-eclosion neurogenesis, and understanding their functional relevance, will provide key insights into how environmental information is stored during post-eclosion development.

Conclusions

Olfactory processing and associative olfactory memory have been commonly regarded as the principal function of the insect MB. This case study in *Heliconius* suggests that an increased behavioral requirement for spatial memory can drive an enlargement of the MB. Our volumetric analyses uncover both an extensive phylogenetic increase in MB size, and extensive ontogenetic size plasticity with a strong experience-dependent component. Both processes may be linked to the derived foraging behavior of *Heliconius*, which relies on allocentric memory of pollen resources (Gilbert, 1975; Sivinski, 1989). When placed together with evidence from earlier studies, our findings identify the insect MB as a likely neuronal substrate of allocentric place memory. This hypothesis must now be further confirmed in wider comparative analyses, tested explicitly in behavioral experiments, and tied to the neuronal changes that underpin changes in MB size and the consequences for circuit function.

Acknowledgments

The authors are grateful to Adriana Tapia, Moises Abanto, William Wcislo, Owen McMillan, Chris Jiggins, and the Smithsonian Tropical Research Institute for assistance, advice, and the use of the *Heliconius* insectaries at Gamboa, Panama, and the Ministerio del Ambiente for permission to collect butterflies in Panama. We also thank Judith Mank's research group at UCL for helpful advice and feedback, and the UCL Imaging Facility for help with confocal microscopy. Finally, we acknowledge the robust and detailed criticism of an anonymous reviewer that greatly improved this manuscript.

Conflict of interest statement

The authors declare no conflict of interest.

Role of authors

All authors read and approved the final manuscript. Study conception: SHM. Study design and preliminary experiments: SHM, RMM, SRO. Fieldwork and insectary rearing: SHM, RMM. Dissections, acquisition of data, analysis, interpretation and initial manuscript draft: SHM. Final interpretation and drafting: SHM, RMM, SRO.

Literature cited

Barton RA. 1998. Visual specialization and brain evolution in primates. Proc Biol Sci 265:1933–1937.

Barton RA, Purvis A, Harvey PH. 1995. Evolutionary radiation of visual and olfactory brain systems in primates, bats and insectivores. Philos Trans R Soc Lond B Biol Sci 348:381–92.

Barton RA, Harvey PH. 2000. Mosaic evolution of brain structure in mammals. Nature 405(6790): 1055-1058.

Beltrán M, Jiggins CD, Brower AVZ, Bermingham E, Mallet J. 2007. Do pollen feeding , pupal-mating and larval gregariousness have a single origin in *Heliconius* butterflies? Inferences from multilocus DNA sequence data. Biol J Linnean Soc 92(2):221–239.

Benson WW. 1972. Natural selection for Miillerian mimicry in *Heliconius erato* in Costa Rica. Science (80-) 176:936–939.

Bender JA, Pollack AJ, Ritzmann RE. 2010. Neural activity in the central complex of the insect brain is linked to locomotor changes. Curr Biol. 20(10):921-6.

Berg BG, Galizia CG, Brandt R, Mustaparta H. 2002. Digital atlases of the antennal lobe in two species of tobacco budworm moths, the Oriental *Helicoverpa assulta* (male) and the American *Heliothis virescens* (male and female). J Comp Neurol 446:123–134.

Boeckh J, Boeckh V. 1979. Threshold and odor specificity of pheromone-sensitive neurons in the deutocerebrum of *Antheraea pernyi* and *A. polyphemus* (Saturnidae). J Comp Physiol A 132:235–242.

Boggs CL, Smiley JT, Gilbert LE. 1981. Patterns of pollen exploitation by *Heliconius* butterflies. Oecologia 48:284–289.

Brandt R, Rohlfing T, Rybak J, Krofczik S, Maye A, Westerhoff M, Hege H-C, Menzel R. 2005. Three-dimensional average-shape atlas of the honeybee brain and its applications. J Comp Neurol 492:1–19.

Briscoe AD, Macias-Muñoz A, Kozak KM, Walters JR, Yuan F, Jamie GA, Martin SH, Dasmahapatra KK, Ferguson LC, Mallet J, Jacquin-Joly E, Jiggins CD.

2013. Female behaviour drives expression and evolution of gustatory receptors in butterflies. PLoS Genet 9:e1003620.

Brown KS. 1981. The biology of *Heliconius*. Annu Rev Entomol 26:427–457.

Carlsson MA, Schäpers A, Nässel DR, Janz N. 2013. Organization of the olfactory system of nymphalidae butterflies. Chem Senses 38:355–67.

Cayre M, Strambi C, Charpin P, Augier R, Meyer MR, Edwards JS, Strambi A. 1996. Neurogenesis in adult insect mushroom bodies. 310:300–310.

Chittka L, Niven J. 2009. Are Bigger Brains Better? Curr Biol 19:R995–R1008.

Cohen J. 1988. Statistical power analysis for the behavioral sciences. 2nd ed. Hillsdale, NJ.: Lawrence Earlbaum Associates.

Dasmahapatra KK, Walters JR, Briscoe AD, Davey JW, Whibley A, Nadeau NJ, Zimin AV, Hughes DST, Ferguson LC, Martin SH, Salazar C, Lewis JJ, Adler S, Ahn S-J, Baker DA, Baxter SW, Chamberlain NL, Chauhan R, Counterman BA, Dalmay T, Gilbert LE, Gordon K, Heckel DG, Hines HM, Hoff KJ, Holland PWH, Jacquin-Joly E, Jiggins FM, Jones RT, Kapan DD, Kersey P, Lamas G, Lawson D, Mapleson D, Maroja LS, Martin A, Moxon S, Palmer WJ, Papa R, Papanicolaou A, Pauchet Y, Ray DA, Rosser N, Salzberg SL, Supple MA, Surridge A, Tenger-Trolander A, Vogel H, Wilkinson PA, Wilson D, Yorke JA, Yuan F, Balmuth AL, Eland C, Gharbi K, Thomson M, Gibbs RA, Han Y, Jayaseelan JC, Kovar C, Mathew T, Muzny DM, Ongeri F, Pu L-L, Qu J, Thornton RL, Worley KC, Wu Y-Q, Linares M, Blaxter ML, Ffrench-Constant RH, Joron M, Kronforst MR, Mullen SP, Reed RD, Scherer SE, Richards S, Mallet J, Owen McMillan W, Jiggins CD. 2012. Butterfly genome reveals promiscuous exchange of mimicry adaptations among species. Nature 487:94–8.

Dreyer D, Vitt H, Dippel S, Goetz B, El Jundi B, Kollmann M, Huetteroth W, Schachtner J. 2010. 3D standard brain of the Red Flour Beetle *Tribolium castaneum*: A tool to study metamorphic development and adult plasticity. Front Syst Neurosci 4:3.

Dufour M-C, Gadenne C. 2006. Adult neurogenesis in a moth brain. J Comp Neurol 495(5):635–643.

Dunlap-Pianka H, Boggs CL, Gilbert LE. 1977. Ovarian dynamics in heliconiine butterflies: programmed senescence versus eternal youth. Science (80-) 197:487–490.

Durst C, Eichmüller S, Menzel R. 1994. Development and experience lead to increased volume of subcompartments of the honeybee mushroom body. Behav Neural Biol 62:259–263.

Edgar RC. 2004. MUSCLE: multiple sequence alignment with high accuracy and high throughput. Nucleic Acids Res 32:1792–7.

911 Ehrlich PR, Gilbert LE. 1973. Population structure and dynamics of the Tropical
912 butterfly *Heliconius ethilla*. Biotropica 5:69–82.

913 Estrada C, Jiggins CD. 2002. Patterns of pollen feeding and habitat preference among
914 *Heliconius* species. Ecol Entomol 27:448–456.

915 Fahrbach SE, Farris SM, Sullivan JP, Robinson GE. 2003. Limits on volume changes
916 in the mushroom bodies of the honey bee brain. J Neurobiol 57:141–151.

917 Fahrbach SE, Giray T, Robinson GE. 1995. Volume changes in the mushroom bodies
918 of adult honey bee queens. Neurobiol Learn Mem 63:181–191.

919 Fahrbach SE, Moore D, Capaldi EA, Farris SM, Robinson GE. 1998. Experience-
920 expectant plasticity in the mushroom bodies of the honeybee. Learn Mem 5:115–
921 123.

922 Farris SM, Roberts NS. 2005. Coevolution of generalist feeding ecologies and
923 gyrencephalic mushroom bodies in insects. Proc Natl Acad Sci U S A
924 102:17394–17399.

925 Farris SM, Robinson GE, Fahrbach SE. 2001. Experience- and age-related outgrowth
926 of intrinsic neurons in the mushroom bodies of the adult worker honeybee. J
927 Neurosci 21:6395–6404.

928 Farris SM, Schulmeister S. 2011. Parasitoidism, not sociality, is associated with the
929 evolution of elaborate mushroom bodies in the brains of hymenopteran insects.
930 Proc Biol Sci 278:940–951.

931 Farris SM. 2005. Evolution of insect mushroom bodies: old clues, new insights.
932 Arthropod Struct Dev 34:211–234.

933 Farris SM. 2008. Tritocerebral tract input to the insect mushroom bodies. Arthropod
934 Struct Dev 37:492–503.

935 Farris SM. 2013. Evolution of complex higher brain centers and behaviors: behavioral
936 correlates of mushroom body elaboration in insects. Brain Behav Evol 82:9–18.

937 Finkbeiner SD. 2014. Communal roosting in *Heliconius* butterflies (nymphalidae):
938 roost recruitment, establishment, fidelity, and resource use trends based on age
939 and sex. J Lepid Soc 68:10–16.

940 Gilbert LE. 1972. Pollen feeding and reproductive biology of *Heliconius* butterflies.
941 Proc Natl Acad Sci U S A 69:1403–1407.

942 Gilbert LE. 1975. Ecological consequences of a coevolved mutualism between
943 butterflies and plants. In: Gilbert LE, Raven P, editors. Coevolution of animals
944 and plants. p 210–240.

945 Gilbert LE. 1993. An evolutionary food web and its relationship to Neotropical
946 biodiversity. In: Barthlott W, Naumann CM, Schmidt-Loske K, Schuchmann

KL, editors. Animal-Plant Interactions in Tropical Environments. Zoologisches Forschungsinstitut und Museum Alexander Koenig, Bonn, Germany. p 17–28.

Godenschwege TA, Reisch D, Diegelmann S, Eberle K, Funk N, Heisenberg M, Hoppe V, Hoppe J, Klagges BRE, Martin JR, Nikitina EA, Putz G, Reifegerste R, Reisch N, Rister J, Schaupp M, Scholz H, Schwärzel M, Werner U, Zars TD, Buchner S, Buchner E. 2004. Flies lacking all synapsins are unexpectedly healthy but are impaired in complex behaviour. Eur J Neurosci 20:611–622.

Greenacre MJ. 2010. Biplots in practice. Fundacion BBVA.

Gronenberg W, Heeren S, Hölldobler B. 1996. Age-dependent and task-related morphological changes in the brain and the mushroom bodies of the ant *Camponotus floridanus*. J Exp Biol 199:2011–9.

Gronenberg W, Hölldobler B. 1999. Morphologic representation of visual and antennal information in the ant brain. J Comp Neurol 412:229–240.

Gronenberg W. 2001. Subdivisions of hymenopteran mushroom body calyces by their afferent supply. J Comp Neurol 435:474–489.

Heinrich B. 1979. Resource heterogeneity and patterns of movement in foraging bumblebees. Oecologia 40:235–245.

Heinze S, Florman J, Asokaraj S, El Jundi B, Reppert SM. 2013. Anatomical basis of sun compass navigation II: the neuronal composition of the central complex of the monarch butterfly. J Comp Neurol 521:267–98.

Heinze S, Reppert SM. 2012. Anatomical basis of sun compass navigation I: the general layout of the monarch butterfly brain. J Comp Neurol 520:1599–628.

Hofbauer A, Ebel T, Waltenspiel B, Oswald P, Chen Y, Halder P, Biskup S, Lewandrowski U, Winkler C, Sickmann A, Buchner S, Buchner E. 2009. The Wuerzburg hybridoma library against *Drosophila* brain. J Neurogenet 23:78–91.

Homberg U. 1984. Processing of antennal information in extrinsic mushroom body neurons of the bee brain. J Comp Physiol A Neuroethol Sens Neural Behav Physiol:825–836.

Huber R, van Staaden MJ, S K Les, Liem KF. 1997. Microhabitat use, trophic patterns, and the evolution of brain structure in African Cichlids. Brain Behav Evol 50:167–182.

Huetteroth W, Schachtner J. 2005. Standard three-dimensional glomeruli of the *Manduca sexta* antennal lobe: a tool to study both developmental and adult neuronal plasticity. Cell Tissue Res 319:513–24.

Ito K, Shinomiya K, Ito M, Armstrong JD, Boyan G, Hartenstein V, Harzsch S, Heisenberg M, Homberg U, Jenett A, Keshishian H, Restifo LL, Rössler W,

983 Simpson JH, Strausfeld NJ, Strauss R, Vosshall LB. 2014. A systematic
984 nomenclature for the insect brain. Neuron 81:755–765.

985 Janzen ADH. 1971. Euglossine bees as long-distance pollinators of Tropical plants.
986 Science (80-) 171:203–205.

987 Jones BM, Leonard AS, Papaj DR, Gronenberg W. 2013. Plasticity of the worker
988 bumblebee brain in relation to age and rearing environment. Brain Behav Evol
989 82:250–261.

990 Jones F. 1930. The sleeping heliconias of Florida. Nat Hist 30:635–644.

991 Jones TA, Donlan NA, O'Donnell S. 2009. Growth and pruning of mushroom body
992 Kenyon cell dendrites during worker behavioral development in the paper wasp,
993 Polybia aequatorialis (Hymenoptera: Vespidae). Neurobiol Learn Mem 92:485–
994 495.

995 El Jundi B, Huetteroth W, Kurylas AE, Schachtner J. 2009. Anisometric brain
996 dimorphism revisited: Implementation of a volumetric 3D standard brain in
997 *Manduca sexta*. J Comp Neurol 517:210–25.

998 Kazawa T, Namiki S, Fukushima R, Terada M, Soo K, Kanzaki R. 2009. Constancy
999 and variability of glomerular organization in the antennal lobe of the silkmoth.
1000 Cell Tissue Res 336:119–36.

1001 Kerpel SM, Moreira GRP. 2005. Absence of learning and local specialization on host
1002 plant selection by *Heliconius erato*. J Insect Behav 18:433–452.

1003 Kinoshita M, Shimohigasshi M, Tominaga Y, Arikawa K, Homberg U. 2015.
1004 Topographically distinct visual and olfactory inputs to the mushroom body in the
1005 Swallowtail Butterfly, *Papilio xuthus*. J Comp Neurol 523:162–182.

1006 Klagges BR, Heimbeck G, Godenschwege TA, Hofbauer a, Pflugfelder GO,
1007 Reifegerste R, Reisch D, Schaupp M, Buchner S, Buchner E. 1996. Invertebrate
1008 synapsins: a single gene codes for several isoforms in *Drosophila*. J Neurosci
1009 16:3154–65.

1010 Kozak KM, Wahlberg N, Dasmahapatra KK, Mallet J, Jiggins CD. 2015. Multilocus
1011 species trees show the recent adaptive radiation of the mimetic *Heliconius*
1012 butterflies. Syst Biol. 64 (3): 505-524.

1013 Krenn HW, Penz CM. 1998. Mouthparts of *Heliconius* butterflies (Lepidoptera :
1014 Nymphalidae): A search for anatomical adaptations to pollen-feeding behavior.
1015 Int J Insect Morphol Embryol 27:301–309.

1016 Kühn-Bühlmann S, Wehner R. 2006. Age-dependent and task-related volume changes
1017 in the mushroom bodies of visually guided desert ants, *Cataglyphis bicolor*. J
1018 Neurobiol 66:511–521.

1019 Kurylas AE, Rohlfing T, Krofczik S, Jenett A, Homberg U. 2008. Standardized atlas
1020 of the brain of the desert locust, *Schistocerca gregaria*. Cell Tissue Res
1021 333:125–45.

1022 Kvello P, Løfaldli BB, Rybak J, Menzel R, Mustaparta H. 2009. Digital, three-
1023 dimensional average shaped atlas of the *Heliothis virescens* brain with integrated
1024 gustatory and olfactory neurons. Front Syst Neurosci 3:14.

1025 Lent DD, Pinter M, Strausfeld NJ. 2007. Learning with half a brain. Dev Neurobiol
1026 67:740–751.

1027 Li Y, Strausfeld NJ. 1999. Multimodal efferent and recurrent neurons in the medial
1028 lobes of cockroach mushroom bodies. J Comp Neurol 409:647–63.

1029 Maleszka J, Barron AB, Helliwell PG, Maleszka R. 2009. Effect of age, behaviour
1030 and social environment on honey bee brain plasticity. J Comp Physiol A
1031 Neuroethol Sensory, Neural, Behav Physiol 195:733–740.

1032 Mallet J. 1980. A laboratory study of gregarious roosting in the butterfly *Heliconius*
1033 *melpomene*. MSc Thesis, University of Newcastle-upon-Tyne.

1034 Mallet J. 1986. Gregarious roosting and home range in *Heliconius* butterflies. Natl
1035 Geogr Res. 2(2): 198-215

1036 Mares S, Ash L. 2005. Brain allometry in bumblebee and honey bee workers.
1037 2005:50–61.

1038 Masante-Roca I, Gadenne C, Anton S. 2005. Three-dimensional antennal lobe atlas of
1039 male and female moths, *Lobesia botrana* (Lepidoptera: Tortricidae) and
1040 glomerular representation of plant volatiles in females. J Exp Biol 208:1147–59.

1041 Menzel R. 2014. The insect mushroom body, an experience-dependent recoding
1042 device. J Physiol Paris 108:84–95.

1043 Mizunami M, Weibrecht JM, Strausfeld NJ. 1998. Mushroom bodies of the
1044 cockroach: their participation in place memory. J Comp Neurol 402:520–537.

1045 Montgomery SH, Ott SR. 2015. Brain composition in *Godyris zavaleta*, a diurnal
1046 butterfly, reflects an increased reliance on olfactory information. J Comp Neurol
1047 523:869–891.

1048 Murawski DA, Gilbert LE. 1986. Pollen flow in *Psiguria warscewiczii*: a comparison
1049 of *Heliconius* butterflies and hummingbirds. Oecologia 68:161–167.

1050 Nordlander RH, Edwards JS. 1969. Postembryonic brain development in the monarch
1051 butterfly, *Danaus plexippus plexippus*, L. Wilhelm Roux' Arch 162:197–217.

1052 Van Nouhuys S, Kaartinen R. 2008. A parasitoid wasp uses landmarks while
1053 monitoring potential resources. Proc Biol Sci 275:377–385.

1054 O'Brien DM, Boggs CL, Fogel ML. 2003. Pollen feeding in the butterfly *Heliconius*
1055 charitonia: isotopic evidence for essential amino acid transfer from pollen to
1056 eggs. Proc Biol Sci 270:2631–2636.

1057 Ott SR, Rogers SM. 2010. Gregarious desert locusts have substantially larger brains
1058 with altered proportions compared with the solitarious phase. Proc Biol Sci
1059 277:3087–96.

1060 Ott SR. 2008. Confocal microscopy in large insect brains: zinc-formaldehyde fixation
1061 improves synapsin immunostaining and preservation of morphology in whole-
1062 mounts. J Neurosci Methods 172:220–30.

1063 Pagel M. 1999. Inferring the historical patterns of biological evolution. Nature
1064 401:877–84.

1065 Penz CM, Krenn HW. 2000. Behavioral adaptations to pollen-feeding in *Heliconius*
1066 butterflies (Nymphalinae, Heliconiinae): An experiment using *Lantana* flowers.
1067 J Insect Behav 13 :865–880.

1068 Pfeiffer K, Homberg U. 2014. Organization and functional roles of the central
1069 complex in the insect brain. Annu Rev Entomol 59:165–84.

1070 Rein K, Zöckler M, Mader MT, Grübel C, Heisenberg M. 2002. The *Drosophila*
1071 standard brain. Curr Biol 12:227–31.

1072 Renwick JAA, Chew FS. 1994. Oviposition behavior in Lepidoptera. Annu Rev
1073 Entomol 39:377–400.

1074 Rø H, Müller D, Mustaparta H. 2007. Anatomical organization of antennal lobe
1075 projection neurons in the moth *Heliothis virescens*. J Comp Neurol 500:658–75.

1076 Rosenheim JA. 1987. Host location and exploitation by the cleptoparasitic wasp
1077 *Argochrysis armilla*: the role of learning (Hymenoptera: Chrysididae). Behav
1078 Ecol Sociobiol 21:401–406.

1079 Rospars JP. 1983. Invariance and sex-specific variations of the glomerular
1080 organization in the antennal lobes of a moth, *Mamestra brassicae*, and a
1081 butterfly, *Pieris brassicae*. J Comp Neurol 220:80–96.

1082 Salcedo C. 2011. Pollen preference for *Psychotria sp*. is not learned in the passion
1083 flower butterfly, *Heliconius erato*. J Insect Sci 11:25.

1084 Schildberger K. 1983. Local interneurons associated with the mushroom bodies and
1085 the central body in the brain of *Acheta domesticus*. Cell Tissue Res 230:573–
1086 586.

1087 Schoonhoven LM. 1968. Chemosensory bases of host plant selection. Annu Rev
1088 Entomol 13:115–136.

1089 Silva AK, Gonçalves GL, Moreira GRP. 2014. Larval feeding choices in heliconians:
1090 Induced preferences are not constrained by performance and host plant
1091 phylogeny. Anim Behav 89:155–162.

1092 Sivan E, Kopell N. 2004. Mechanism and circuitry for clustering and fine
1093 discrimination of odors in insects. Proc Natl Acad Sci U S A 101:17861–17866.

1094 Sivinski J. 1989. Mushroom body development in nymphalid butterflies: A correlate
1095 of learning? J Insect Behav 2:277–283.

1096 Sjöholm M, Sinakevitch I, Ignell R, Strausfeld NJ, Hansson BS. 2005. Organization
1097 of Kenyon cells in subdivisions of the mushroom bodies of a lepidopteran insect.
1098 J Comp Neurol 491:290–304.

1099 Skiri HT, Rø H, Berg BG, Mustaparta H. 2005. Consistent organization of glomeruli
1100 in the antennal lobes of related species of heliothine moths. J Comp Neurol
1101 491:367–80.

1102 Smith AR, Seid M a, Jiménez LC, Wcislo WT. 2010. Socially induced brain
1103 development in a facultatively eusocial sweat bee *Megalopta genalis*
1104 (Halictidae). Proc Biol Sci 277:2157–2163.

1105 Snell-Rood EC, Papaj DR, Gronenberg W. 2009. Brain size: a global or induced cost
1106 of learning? Brain Behav Evol 73:111–28.

1107 Sterling P, Laughlin S. 2015. Principles of efficient wiring. In: Principles of Neural
1108 Design. London, England: MIT Press. p 363–397.

1109 Strauss R. 2002. The central complex and the genetic dissection of locomotor
1110 behaviour. Curr Op Neurobiol. 12(6):633-8.
1111
1112 Strausfeld NJ, Okamura JY. 2007. Visual system of calliphorid flies: organization of
1113 optic glomeruli and their lobula complex efferents. J Comp Neurol. 500(1):166-88.

1114 Strausfeld NJ, Sinakevitch I, Brown SM, Farris SM. 2009. Ground plan of the insect
1115 mushroom body: functional and evolutionary implications. J Comp Neurol
1116 513:265–91.

1117 Strausfeld NJ. 2002. Organization of the honey bee mushroom body: representation of
1118 the calyx within the vertical and gamma lobes. J Comp Neurol 450:4–33.

1119 Striedter GF. 2005. Principles of Brain Evolution. Sunderland, MA: Sinauer.

1120 Tamura K, Peterson D, Peterson N, Stecher G, Nei M, Kumar S. 2011. MEGA5:
1121 molecular evolutionary genetics analysis using maximum likelihood,
1122 evolutionary distance, and maximum parsimony methods. Mol Biol Evol
1123 28:2731–9.

1124 Team RDC. 2008. R: A language and environment for statistical computing. R
1125 Foundation for Statistical Computing, Vienna, Austria. ISBN 3-900051-07-0.
1126 URL http//wwwR-project.org.

1127 Trautwein MD, Wiegmann BM, Beutel R, Kjer KM, Yeates DK. 2012. Advances in
1128 insect phylogeny at the dawn of the postgenomic era. Annu Rev Entomol
1129 57:449–468.

1130 Turner JRG. 1971. Experiments on the demography of tropical butterflies. II.
1131 Longevity and home-range behaviour in *Heliconius erato*. Biotropica 3:21–31.

1132 Turner JRG. 1981. Adaptation and evolution in *Heliconius*: a defense of
1133 NeoDarwinism. Annu Rev Ecol Syst 12:99–121.

1134 Utz S, Huetteroth W, Vomel M, Schachtner J. 2008. Mas-allatotropin in the
1135 aeveloping antennal lobe of the Sphinx Moth *Manduca sexta*: distribution, time
1136 course, developmental regulation, and colocalization withother Nneuropeptides.
1137 Dev Neurobiol 68:123–142.

1138 Warren AD, Davis KJ, Strangeland EM, Pelham JP, Grishin NV. 2013. Illustrated
1139 lists of American butterflies. http://butterfliesofamerica.com

1140 Warton DI, Duursma RA, Falster DS, Taskinen S. 2012. smatr 3- an R package for
1141 estimation and inference about allometric lines. Methods Ecol Evol 3:257–259.

1142 Wei H, el Jundi B, Homberg U, Stengl M. 2010. Implementation of pigment-
1143 dispersing factor-immunoreactive neurons in a standardized atlas of the brain of
1144 the cockroach *Leucophaea maderae*. J Comp Neurol 518:4113–33.

1145 Withers G, Day NF, Talbot EF, Dobson HEM, Wallace CS. 2008. Experience-
1146 dependent plasticity in the mushroom bodies of the solitary bee *Osmia lignaria*
1147 (Megachilidae). Dev Neurobiol 68:73–82.

1148 Withers GS, Fahrbach SE, Robinson GE. 1993. Selective neuroanatomical plasticity
1149 and division of labour in the honeybee. Nature 364:238–40.

1150 Wolf H, Wehner R. 2000. Pinpointing food sources: olfactory and anemotactic
1151 orientation in desert ants, *Cataglyphis fortis*. 868:857–868.

1152 Zars T. 2000. Behavioral functions of the insect mushroom bodies. Curr Opin
1153 Neurobiol 10:790–795.

1154

1155

1156

1157

1158

Abbreviations

AL	antennal lobe
ALH	antennal lobe hub
AME	accessory medulla
AN	antennal nerve
AOTU	anterior optic tubercle
CA	calyx of mushroom body
CB	central body
CBL	lower division of central body
CBR	central brain
CBU	upper division of central body
CX	central complex
DMSO	dimethyl suphoxide
GL	glomeruli
GNG	gnathal ganglia
HBS	HEPES-buffered saline
IME	inner medulla
iRim	inner rim of the lamina
KC	Kenyon cell
LBM	lobes mass of the mushroom body
LA	lamina
LAL	lateral accessory lobes
LO	lobula
LOP	lobula plate
LU	lower unit of AOTU
MB	mushroom body
ME	medulla
MGC	macro-glomeruli complex
NGS	normal goat serum
NO	noduli
NU	nodular unit of AOTU
OME	outer medulla
OL	optic lobe
OR	olfactory receptor
OS	optic stalk
PA	pyrrolizidine alkaloids
PB	protocerebral bridge
PC	principal component
PED	pedunculus of mushroom body
POTU	posterior optic tubercle
rCBR	(un-segmented) rest of central brain
SP	strap of AOTU
UU	upper unit of AOTU
vLO	ventral lobe of the LO
ZnFA	Zinc-Formaldehyde solution

Figure Legends

Figure 1: Overview of the anatomy of the *Heliconius* brain.

3D models of *H. erato* (**A1–G1**) and *H. hecale* (**A2–G2**). **B1–D1** and **B2–D2:** Volume rendering of synapsin immunofluorescence showing the surface morphology of the brain neuropil from the anterior (B1/B2), posterior (C1/C2), and dorsal (D1/D2) view. **E1–G1** and **E2–G2:** Surface reconstructions of the major neuropil compartments from the anterior (E1/E2), posterior (F1/F2), and dorsal (G1/G2) view. Neuropil in yellow-orange: visual neuropil, green: central complex, blue: antennal lobes, red: mushroom bodies. See Figures 2–4 for further anatomical detail. The individuals displayed are male. Images in A1/A2 are from Warren et al. (2013). Scale bars = 25 mm in A1/A2; 500 µm in B1–D1/B2–D2.

Figure 2: Anatomy of the major visual neuropils.

A: Surface reconstructions of the optic lobe (OL) neuropils viewed from anterior (left image) and posterior (right image). They comprise the lamina (LA), the medulla (ME) and accessory medulla (AME), the lobula (LO), the lobula plate (LOP) and the ventral lobe of the lobula (vLO). **B:** Surface reconstruction of the vLO viewed along the anterior-posterior axis (top) and an anterior view (bottom)**. C:** Surface reconstruction of the anterior optic tubercle (AOTU)**. D–J:** Synapsin immunofluorescence in single confocal sections of the OL of *H. hecale*. **D:** Horizontal section showing four major OL neuropils (LA, ME, LO, LOP). **E:** Frontal section showing the inner rim (iRim) of the LA, a thin layer on its inner surface that is defined by intense synapsin immunofluorescence. Synapsin immunostaining also reveals the laminated structure of the ME with two main subdivisions, the outer and inner medulla (OME, IME). **F:** vLO is located medially to the LO; frontal section, the central brain (CBR) occupies the left half of the frame. **G,H:** Frontal sections showing a small, irregular neuropil (ir) observed running from the anterior-ventral boundary of the AME as in *D. plexippus* (Heinze and Reppert, 2012). All images are from male *H. hecale.* Scale bars = 500 µm in A; 50 µm in B-C, G-H; 100 µm in D-F.

Figure 3: Anatomy of the antennal lobe

A: 3D reconstruction of individual antennal lobe (AL) glomeruli superimposed on a volume rendering of the anterior surface of the central brain. **B:** Synapsin immunofluorescence in a single frontal confocal section showing the glomeruli (GL) surrounding the fibrous neuropil of the AL hub (ALH). Images A–B are from male *H. hecale*. **C,D:** Allometric grade-shifts between GL (circles) or ALH (triangles) volume and unsegmented central brain volume (C), and between GL and ALH volume (D) in *G. zavaleta* (solid blue), *H. erato* (black filled with red) and *H. hecale* (orange filled with yellow). Scale bars = 200 μm in A, 100 μm in B

Figure 4: Anatomy of the central complex

A1/A2: Surface reconstruction of the central complex (CX) from an anterolateral (A1) and oblique posteroventral (A2) view, showing the upper and lower subunit of the central body (CBU, CBL), the noduli (NO), the protocerebral bridge (PB) and posterior optic tubercles (POTU). **B–G:** Synapsin immunofluorescence in single confocal sections. **B:** Horizontal section showing the upper and lower subunit of the CB in relation to the antennal lobes (AL) and the calyx (CA) and pedunculus (PED) of the mushroom body. **C,D:** Frontal confocal sections at the level of the CBL (C) and CBU (D); the CB subunits are flanked by the profiles of the vertically running PED on either side. **E:** Frontal section showing the location of the PB ventrally to the CA **F:** POTU positioned ventrally to the CA in a frontal section. **G:** Frontal section showing position of the paired NO ventrally to CBL and CBU. All images are from a male *H. hecale.* Scale bars = 100 μm in B–D, G; 50 μm in E,F.

Figure 5: Anatomy of the mushroom body

A–C: Surface reconstruction of the mushroom body (BM) viewed orthogonal to the anterior-posterior axis from a medial vantage point level with the pedunculus (A); from anterior (B); and from posterior (C). The main components are the calyx (CA, dark red), the pedunculus (PED), and the lobes, which are largely fused into a single mass (LBM); PED and LBM are shown in bright red. A Y-tract (YT), shown in magenta, runs parallel and slightly medial to PED. **D–O:** Synapsin immunofluorescence in individual confocal sections. **D:** anterior view of the central brain showing the LBM, an asterisk indicates what is most likely the vertical lobe,

otherwise the individual lobes and loblets of the LBM are fused. **E:** Frontal section at a posterior level near the end of the PED, showing the profiles of the CA with their zonation into an outer and a medial ring. **F,G** and **J,K**: Horizontal confocal sections through the central brain at increasing depths from dorsal towards ventral, showing MB structure in relation to neighboring neuropil: the anterior optic tubercle (AOTU in F,G); the antennal lobe (AL in G,J); and the central body upper division (CBU in K). **H:** An example of a female *H. erato* where the CA is deformed due expansion into the optic lobe and constriction (labeled *con.*) at the optic stalk by the neural sheath surrounding the brain. **I:** Pitted surface of the CA in a very posterior tangential horizontal section. The pitting is related to what appear to be columnar domains within the CA neuropil (*cf.* CA in J,K,M). **L:** Areas of intense synapsin staining in the optic stalk (OS); LO, lobula; vLO, optic glomerular complex. **M:** Frontal section near the base of the CA showing a satellite neuropil (labeled *sat.*) located near to the PED. **N:** YT runs parallel with, and dorsally and slightly medially to PED; both are seen in profile in this frontal section. **O:** A fiber bundle (fb) connected to the AOTU running near the junction between PED and LBM. With the exception of I, all images are from a male *H. hecale.* Scale bars A-G, J-K = 200 μm, H-I, L-O = 100 μm.

Figure 6: Divergence in brain structure across Lepidoptera, and in mushroom body size across insects.

A: Phylogenetic relationships of Lepidoptera (red branches) and other insects (grey branches) for which directly comparable data are available. Branches are not drawn proportional to divergence dates, numbers refer to labels in panel E. **B,C:** Principal Component analysis of segmented neuropil volumes, corrected for allometric scaling with the unsegmented central brain and for phylogeny. **B:** analysis using all neuropil. **C:** analysis excluding the optic lobe neuropil. Species data points are indicated by the first letter of their genus and species name: *D.p = Danaus plexippus*; *H.e = Heliconius erato*; *H.h = H. hecale*; *G.z = Godyris zavaleta*; *H.v = Heliothis virescens*; *M.s = Manduca sexta*. **D:** The proportion of the central brain occupied by CA (dark red) and PED and the MB lobes (light red) in four butterflies, and two other insects with fully comparable data. **E:** Across a wider sample of insects (shown in A), when expressed as a percentage of total volume of OL, AL, CB and MB, *Apis mellifera* (solid blue) and *Heliconius* (solid red) stand out as having expanded MBs, correcting for the size of the optic neuropil, compared to other Lepidoptera (unfilled red circles) and other

insects (unfilled blue circles). The line was fitted by PGLS. All insect images in A are from Wikimedia commons and were released under the Creative Commons License, except *Heliconius* (see Fig. 1).

Figure 7: Age and environment dependent growth of brain components

A: Comparisons of raw volumes of total neuropil, total OL neuropil, and total central brain neuropil between wild-caught, old and young insectary-reared individuals of *H. erato* (A1) and *H. hecale* (A2). Significance of pair-wise comparisons is shown along the x-axis (young-old = orange; old-wild = dark red; n.s. = $p>0.05$, * = $p<0.05$, ** = $p<0.01$, *** = $p < 0.001$). **B:** Allometric scaling of LOP in *H. erato*. **C:** Allometric scaling of PB in *H. erato*. **D:** Allometric scaling of vLO in *H. hecale*. **E:** Allometric scaling of CB in *H. hecale*. Note that in D and E the shifts in allometry occur along the x-axis, this is explained by the large difference in unsegmented central brain volume observed between wild-caught and old insectary-reared individuals in *H. hecale* as displayed in D.

Figure 8: Age and environment dependent growth of the mushroom bodies

Surface reconstruction of the mushroom body viewed along the anterior-posterior axis for wild-caught, old and young insectary-reared individuals of *H. erato* (**A1**) and *H. hecale* (**A2**). Representative individuals were chosen as those closest to the group mean volume. Scale bar = 200 μm. **B1-C1/B2-C2:** allometric relationships between PED+LBM (B1/B2), or CA (C1/C2), and the volume of the unsegmented, rest of central brain (rCBR) for *H. erato* (B1/C1) and *H. hecale* (B2/C2). Data for wild caught individuals are in green, data for old insectary-reared individuals in dark blue, and data for young insectary-reared individuals are in light blue. Allometric slopes for each group are shown, the slope, intercepts and major-axis means are compared in Table 3,4.

Tables

Table 1: Neuropil volumes (in μm^3) and body size of A) *H. erato* and B) *H. hecale*

Table 2: Loadings on Principal Components Analysis of the relative size of brain components across six Lepidoptera.

Table 3: Comparisons between old (O) and young (Y) insectary-reared individuals for A) *H. erato* and B) *H. hecale.* The tests for differences in allometric slopes (β), intercepts (α) and for major axis shifts are for $\log_{10}$-$\log_{10}$ standardized major axis regressions against rCBR; *r* is a measure of effect size. DI (Direction of Increase) indicates the group with a higher value of α, β or fitted axis mean.

Table 4: Comparisons between wild caught (W) and old insectary-reared individuals for A) *H. erato* and B) *H. hecale.* The tests for differences in allometric slopes (β), intercepts (α) and for major axis shifts are for $\log_{10}$-$\log_{10}$ standardized major axis regressions against rCBR; *r* is a measure of effect size. DI (Direction of Increase) indicates the group with a higher value of α, β or fitted axis mean.

Table 5: Effects of age (A) and environmental experience (B) on scaling relationships between mushroom body components, analyzed by major axis regression of log-transformed volumes. DI (Direction of Increase) indicates the group with a higher value of α, β or fitted axis mean: O = old, W = wild.

Table 1

A) *H. erato*

	wild caught				*old insectary reared*		*young insectary reared*	
	mean (*n* = 10)	**SD**	**Rel. SD (%)**	**% total neuropil**	**mean (*n* = 10)**	**SD**	**mean (*n* = 10)**	**SD**
Body mass (g)	0.093	0.017	19.999	-	0.074	0.014	0.088	0.019
Body length (mm)	23.833	1.426	5.983	-	23.095	1.773	22.671	0.951
Wing span (mm)	71.408	3.278	4.591	-	69.744	4.12	68.786	2.55
LA	7.409E+07	1.052E+07	14.192	13.459	6.95E+07	1.61E+07	5.49E+07	1.25E+07
ME	2.396E+08	3.617E+07	15.094	43.523	2.45E+08	2.76E+07	1.90E+08	3.32E+07
AME	1.633E+05	3.609E+04	22.094	0.030	1.59E+05	4.61E+04	9.77E+04	1.93E+04
LO	2.630E+07	4.203E+06	15.984	4.777	2.79E+07	2.89E+06	2.07E+07	4.32E+06
LOP	1.393E+07	2.083E+06	14.952	2.531	1.35E+07	2.22E+06	1.04E+07	2.07E+06
vLO	1.054E+06	2.400E+05	22.769	0.191	1.05E+06	2.42E+05	8.85E+05	2.26E+05
AL	1.185E+07	2.450E+06	20.671	2.153	1.19E+07	2.49E+06	7.72E+06	1.10E+06
AOTU	2.199E+06	4.535E+05	20.618	0.400	2.26E+06	3.28E+05	1.52E+06	3.27E+05
CA	4.672E+07	9.290E+06	19.886	8.486	4.50E+07	1.22E+07	2.79E+07	5.75E+06
PED	6.043E+06	1.109E+06	18.343	1.098	6.15E+06	1.35E+06	5.57E+06	1.58E+06
LBM	2.267E+07	5.812E+06	25.641	4.118	2.17E+07	4.26E+06	1.28E+07	2.31E+06
CBL	3.017E+05	5.189E+04	17.198	0.055	2.83E+05	6.00E+04	2.24E+05	3.81E+04
CBU	1.180E+06	1.788E+05	15.153	0.214	1.17E+06	2.57E+05	8.90E+05	1.36E+05
NO	2.966E+04	1.146E+04	38.631	0.005	3.09E+04	1.64E+04	3.16E+04	8.46E+03
PB	2.120E+05	4.804E+04	22.658	0.039	1.96E+05	5.04E+04	1.39E+05	2.02E+04
POTU	4.213E+04	9.976E+03	23.681	0.008	4.20E+04	1.43E+04	2.73E+04	7.93E+03
Total CBR	1.954E+08	3.365E+07	17.222	35.490	2.04E+08	2.70E+07	1.39E+08	2.28E+07

B) *H. hecale*

	wild caught				*old insectary reared*		*young insectary reared*	
	mean (*n* = 10)	**SD**	**Rel. SD (%)**	**% total neuropil**	**mean (*n* = 9)**	**SD**	**mean (*n* = 10)**	**SD**
Body mass (g)	0.163	0.025	15.317	-	0.154	0.046	0.171	0.047
Body length (mm)	29.693	3.097	10.431	-	28.189	3.0631	29.206	2.75
Wing span (mm)	88.129	8.004	9.082	-	80.6	7.134	86.34	8.012
LA	9.751E+07	1.826E+07	18.721	13.939	9.39E+07	2.17E+07	9.64E+07	1.50E+07
ME	2.986E+08	5.342E+07	17.888	42.689	2.48E+08	3.81E+07	2.42E+08	3.66E+07
AME	1.660E+05	2.951E+04	17.782	0.024	1.40E+05	2.80E+04	1.38E+05	3.67E+04
LO	3.056E+07	5.630E+06	18.422	4.369	2.80E+07	4.64E+06	2.45E+07	5.06E+06
LOP	1.648E+07	2.972E+06	18.031	2.356	1.45E+07	2.45E+06	1.27E+07	2.53E+06
vLO	1.099E+06	3.396E+05	30.894	0.157	9.93E+05	2.12E+05	9.24E+05	2.10E+05
AL	1.216E+07	2.056E+06	16.905	1.739	1.09E+07	1.34E+06	9.36E+06	1.59E+06
AOTU	2.572E+06	6.144E+05	23.891	0.368	2.30E+06	4.46E+05	2.02E+06	3.76E+05
CA	5.271E+07	1.611E+07	30.569	7.534	3.60E+07	7.49E+06	2.60E+07	7.48E+06
PED	6.680E+06	1.525E+06	22.834	0.955	5.92E+06	1.30E+06	4.91E+06	1.39E+06
LBM	2.421E+07	6.279E+06	25.930	3.461	1.79E+07	3.56E+06	1.32E+07	3.51E+06
CBL	3.109E+05	6.362E+04	20.467	0.044	2.91E+05	7.15E+04	2.47E+05	3.74E+04
CBU	1.093E+06	2.026E+05	18.541	0.156	1.16E+06	2.05E+05	9.65E+05	1.79E+05
NO	4.207E+04	1.713E+04	40.730	0.006	3.34E+04	8.35E+03	3.06E+04	1.28E+04
PB	2.424E+05	5.657E+04	23.335	0.035	2.00E+05	3.09E+04	1.64E+05	1.75E+04
POTU	4.183E+04	1.257E+04	30.057	0.006	3.74E+04	8.47E+03	3.20E+04	8.27E+03
Total CBR	2.551E+08	6.253E+07	24.513	36.465	1.82E+08	2.28E+07	1.50E+08	2.25E+07

Table 2

A) Neuropils in the Central brain only

	Loadings	
	Residuals	
Neuropil	**PC1**	**PC2**
AL	-0.981	-0.045
CBL+CBU	-0.798	0.406
CA	0.962	0.110
PED+LBM	0.952	0.231
AOTU	-0.047	0.966

B) All neuropils

	Loadings	
	Residuals	
Neuropil	**PC1**	**PC2**
AL	0.761	0.619
CBL+CBU	0.671	0.670
CA	-0.961	0.212
PED+LBM	-0.942	0.222
AOTU	0.811	0.024
ME	0.042	-0.949
LO	0.920	-0.354
LOP	0.962	-0.167

Table 3

A) *H. erato*

	Volume			Scaling coefficient (β)			Intercept (α)			Major Axis Shift		
	t_{17}	*p*	*r* (DI)	LR	*p*	*r* (DI)	Wald $\chi 2$	*p*	*r* (DI)	Wald $\chi 2$	*p*	*r* (DI)
LA	2.432	0.026	0.508 (O)	2.019	0.155	-	2.895	0.089	-	13.196	0.000	0.833 (O)
ME	4.118	0.001	0.707 (O)	0.090	0.765	-	1.127	0.288	-	19.405	0.000	1.000 (O)
AME	3.802	0.001	0.678 (O)	3.976	0.046	0.458 (O)	-	-	-	-	-	-
LO	4.173	0.001	0.711 (O)	0.246	0.620	-	1.587	0.208	-	20.284	0.000	1.000 (O)
LOP	3.266	0.005	0.621 (O)	0.523	0.470	-	3.802	0.051	-	19.034	0.000	1.000 (O)
vLO	1.412	0.176	-	0.385	0.535	-	5.694	0.017	0.547 (Y)	10.622	0.001	0.748 (O)
AL	5.080	0.000	0.776 (O)	4.169	0.041	-	0.214	0.644	-	27.584	0.000	1.000 (O)
AOTU	5.192	0.000	0.783 (O)	0.109	0.741	-	0.123	0.726	-	26.321	0.000	1.000 (O)
CA	4.050	0.001	0.701 (O)	3.679	0.055	-	1.607	0.205	-	19.177	0.000	1.000 (O)
PED+LBM	4.806	0.000	0.759 (O)	0.963	0.326	-	0.373	0.541	-	23.250	0.000	1.000 (O)
CBL+CBU	3.272	0.004	0.622 (O)	2.364	0.124	-	1.807	0.179	-	16.530	0.000	0.933 (O)
PB	3.169	0.006	0.609 (O)	5.996	0.014	0.562 (O)	-	-	-	-	-	-
POTU	2.772	0.013	0.558 (O)	1.539	0.215	-	4.124	0.042	0.466 (Y)	14.953	0.000	0.887 (O)
Total CBR	4.192	0.001	0.713 (O)	-	-	-	-	-	-	-	-	-
rCBR	5.771	0.000	0.814 (O)	-	-	-	-	-	-	-	-	-
Total OL	5.076	0.000	0.776 (O)	-	-	-	-	-	-	-	-	-
Total neuropil	5.153	0.000	0.781 (O)	-	-	-	-	-	-	-	-	-

B) *H. hecale*

	Volume			Scaling coefficient (β)			Intercept (α)			Major Axis Shift		
	t_{18}	*p*	*r* (DI)	LR	*p*	*r* (DI)	Wald $\chi 2$	*p*	*r* (DI)	Wald $\chi 2$	*p*	*r* (DI)
LA	-0.424	0.677	-	1.866	0.172	-	11.902	0.001	0.771 (Y)	1.043	0.307	-
ME	0.333	0.743	-	0.494	0.482	-	21.674	0.000	1.000 (Y)	1.971	0.160	-
AME	0.238	0.814	-	0.094	0.759	-	3.044	0.081	-	3.088	0.079	-
LO	1.538	0.141	-	0.002	0.961	-	3.544	0.060	-	4.501	0.034	0.474 (O)
LOP	1.683	0.110	-	0.066	0.797	-	1.577	0.209	-	5.031	0.025	0.502 (O)
vLO	0.617	0.545	-	0.266	0.606	-	4.408	0.036	0.470 (Y)	3.045	0.081	-
						-						
AL	2.418	0.026	0.495 (O)	1.795	0.180	-	2.396	0.122	-	6.451	0.011	0.570 (O)
AOTU	1.496	0.152	-	0.101	0.751	-	2.166	0.141	-	4.656	0.031	0.483 (O)
CA	3.177	0.005	0.599 (O)	0.283	0.595	-	0.104	0.747	-	9.166	0.002	0.677 (O)
PED+LBM	2.707	0.014	0.538 (O)	0.147	0.702	-	0.015	0.902	-	7.594	0.006	0.616 (O)
CBL+CBU	2.218	0.040	0.463 (O)	3.291	0.070	-	0.859	0.354	-	7.221	0.007	0.601 (O)
PB	3.291	0.004	0.613 (O)	1.043	0.307	-	0.172	0.678	-	9.448	0.002	0.687 (O)
POTU	1.494	0.153	-	0.078	0.780	-	0.736	0.391	-	6.292	0.012	0.561 (O)
Total CBR	3.054	0.007	0.584 (O)	-	-	-	-	-	-	-	-	-
rCBR	2.854	0.011	0.558 (O)	-	-	-	-	-	-	-	-	-
Total OL	0.280	0.783	-	-	-	-	-	-	-	-	-	-
Total neuropil	1.082	0.293	-	-	-	-	-	-	-	-	-	-

Table 4

A) *H. erato*

	Volume			Scaling coefficient (β)			Intercept (α)			Major Axis Shift		
	t_{17}	*p*	*r* (DI)	LR	*p*	*r* (DI)	Wald $\chi 2$	*p*	*r* (DI)	Wald $\chi 2$	*p*	*r* (DI)
LA	0.892	0.385	-	3.685	0.055	-	3.605	0.058	-	0.210	0.646	-
ME	-0.426	0.676	-	0.269	0.604	-	2.056	0.152	-	1.269	0.260	-
AME	0.359	0.724	-	5.150	0.023	0.521 (O)	-	-	-	-	-	-
LO	-1.056	0.306	-	0.283	0.595	-	1.004	0.316	-	1.999	0.157	-
LOP	0.430	0.673	-	4.963	0.026	0.511 (O)	-	-	-	-	-	-
vLO	0.116	0.909	-	2.148	0.143	-	2.055	0.152	-	0.848	0.357	-
AL	-0.035	0.972	-	1.695	0.193	-	2.269	0.132	-	0.899	0.343	-
AOTU	-0.490	0.631	-	0.483	0.487	-	1.318	0.251	-	1.456	0.227	-
CA	0.511	0.616	-	5.833	0.016	0.554 (O)	-	-	-	-	-	-
PED+LBM	0.239	0.814	-	0.714	0.398	-	4.418	0.036	0.482 (W)	7.594	0.006	0.632 (W)
CBL+CBU	0.394	0.699	-	4.272	0.039	0.474 (O)	-	-	-	-	-	-
PB	0.845	0.410	-	4.413	0.036	0.482 (O)	-	-	-	-	-	-
POTU	0.196	0.847	-	3.726	0.054	-	2.730	0.098	-	0.905	0.341	-
Total CBR	-0.732	0.474	-	-	-	-	-	-	-	-	-	-
rCBR	-1.787	0.092	-	-	-	-	-	-	-	-	-	-
Total OL	-0.123	0.904	-	-	-	-	-	-	-	-	-	-
Total neuropil	-0.432	0.671	-	-	-	-	-	-	-	-	-	-

B) *H. hecale*

	Volume			Scaling coefficient (β)			Intercept (α)			Major Axis Shift		
	t_{18}	*p*	*r* (DI)	LR	*p*	*r* (DI)	Wald $\chi 2$	*p*	*r* (DI)	Wald $\chi 2$	*p*	*r* (DI)
LA	0.437	0.667	-	6.725	0.010	0.580 (O)	-	-	-	-	-	-
ME	2.293	0.034	0.475 (W)	9.165	0.002	0.677 (O)	-	-	-	-	-	-
AME	1.898	0.074	-	3.728	0.054	-	1.463	0.227	-	8.056	0.005	0.688 (W)
LO	1.017	0.322	-	9.760	0.002	0.699 (O)	-	-	-	-	-	-
LOP	1.609	0.125	-	6.081	0.014	0.551 (O)	-	-	-	-	-	-
vLO	0.614	0.547	-	4.262	0.039	0.462 (O)	-	-	-	-	-	-
AL	1.519	0.146	-	7.095	0.008	0.596 (O)	-	-	-	-	-	-
AOTU	1.088	0.291	-	3.938	0.047	0.444 (O)	-	-	-	-	-	-
CA	3.126	0.006	0.593 (W)	1.657	0.198	-	0.395	0.530	-	10.432	0.001	0.722 (W)
PED+LBM	2.536	0.021	0.513 (W)	3.759	0.053	-	1.603	0.205	-	8.811	0.003	0.664 (W)
CBL+CBU	-0.446	0.661	-	1.665	0.197	-	11.013	0.001	0.742 (O)	2.385	0.122	-
PB	1.919	0.071	-	5.043	0.025	0.502 (O)	-	-	-	-	-	-
POTU	0.551	0.588	-	5.420	0.020	0.521 (O)	-	-	-	-	-	-
Total CBR	3.658	0.002	0.653 (W)	-	-	-	-	-	-	-	-	-
rCBR	3.417	0.003	0.627 (W)	-	-	-	-	-	-	-	-	-
Total OL	1.728	0.101	-	-	-	-	-	-	-	-	-	-
Total neuropil	2.553	0.020	0.516 (W)	-	-	-	-	-	-	-	-	-

Table 5

A) ***Old versus young insectary reared***

		Scaling coefficient (β)			Intercept (α)			Major Axis Shift		
	Components	**LR**	***p***	***r***	**Wald χ2**	***p***	***r***	**Wald χ2**	***p***	***r* (DI)**
H. erato	CA vs. LBM	0.627	0.428	-	2.249	0.134		16.987	0.000	0.946 (O)
	CA vs. PED	1.224	0.269	-	12.457	0.000	0.810	-	-	-
	LBM vs. PED	0.206	0.650	-	29.286	0.000	1.000	-	-	-
H. hecale	CA vs. LBM	0.100	0.752	-	0.058	0.810		8.771	0.003	0.662 (O)
	CA vs. PED	0.376	0.540	-	6.422	0.011	0.567	-	-	-
	LBM vs. PED	0.118	0.731	-	5.462	0.019	0.523	-	-	-

B) ***Wild versus old insectary reared***

		Scaling coefficient (β)			Intercept (α)			Major Axis Shift		
	Components	**LR**	***p***	***r***	**Wald χ2**	***p***	***r***	**Wald χ2**	***p***	***r* (DI)**
H. erato	CA vs. LBM	4.083	0.043	0.464	0.139	0.709	-	0.186	0.667	-
	CA vs. PED	0.311	0.577	-	0.732	0.392	-	0.044	0.834	-
	LBM vs. PED	1.296	0.255	-	0.213	0.645	-	0.011	0.916	-
H. hecale	CA vs. LBM	0.307	0.580	-	0.398	0.528	-	7.901	0.005	0.629 (W)
	CA vs. PED	2.942	0.086	-	7.340	0.007	0.606	-	-	-
	LBM vs. PED	1.553	0.213	-	4.086	0.043	0.452	-	-	-

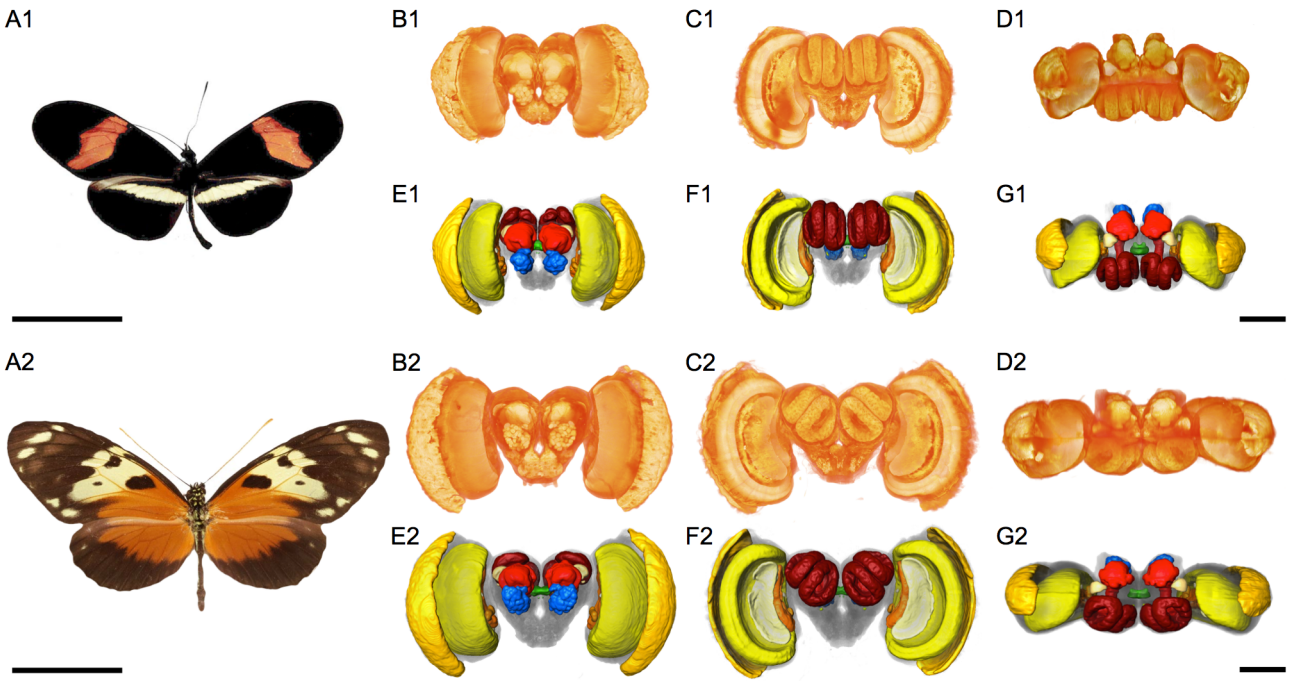
A1
B1
C1
D1
E1
F1
G1
A2
B2
C2
D2
E2
F2
G2

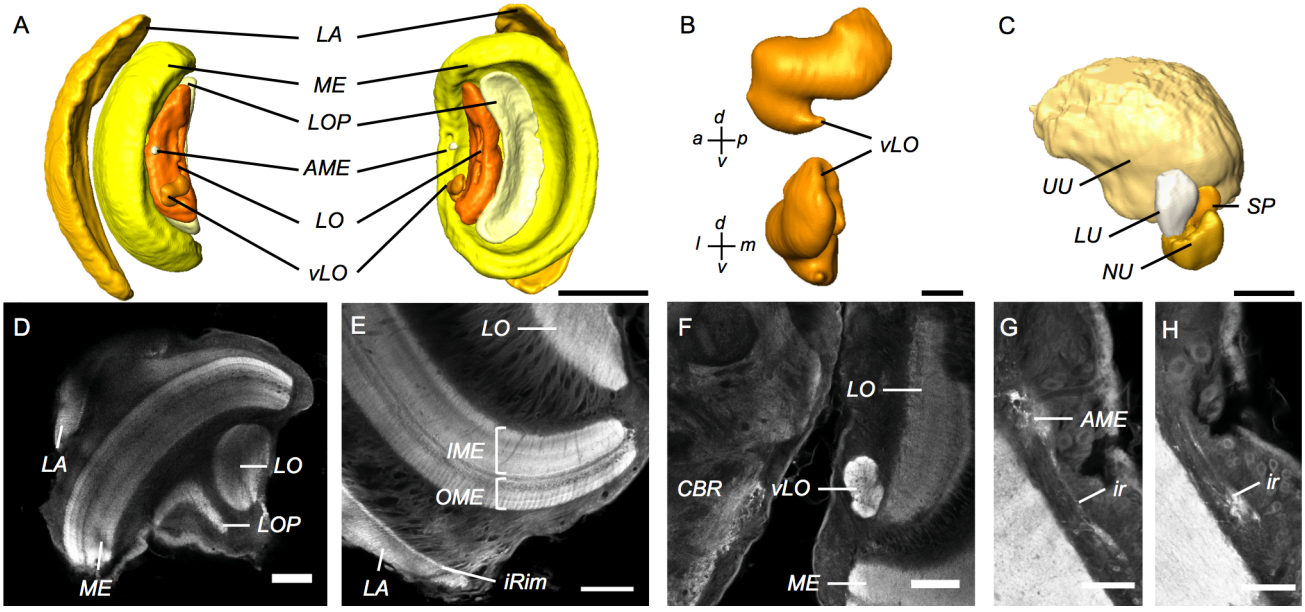
A
LA
ME
LOP
AME
LO
vLO
B
d
a
p
v
vLO
d
l
m
v
C
UU
SP
LU
NU
D
LA
LO
LOP
ME
E
LO
IME
OME
LA
iRim
F
LO
CBR
vLO
ME
G
AME
ir
H
ir

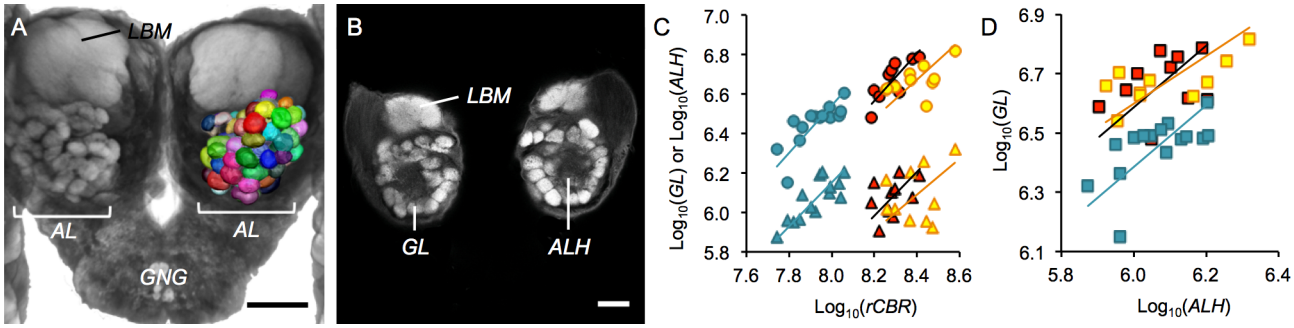
A
LBM
AL
AL
GNG
B
LBM
GL
ALH
C
Log10(GL) or Log10(ALH)
7.0
6.8
6.6
6.4
6.2
6.0
5.8
7.6
7.8
8.0
8.2
8.4
8.6
Log10(rCBR)
D
Log10(GL)
6.9
6.7
6.5
6.3
6.1
5.8
6.0
6.2
6.4
Log10(ALH)

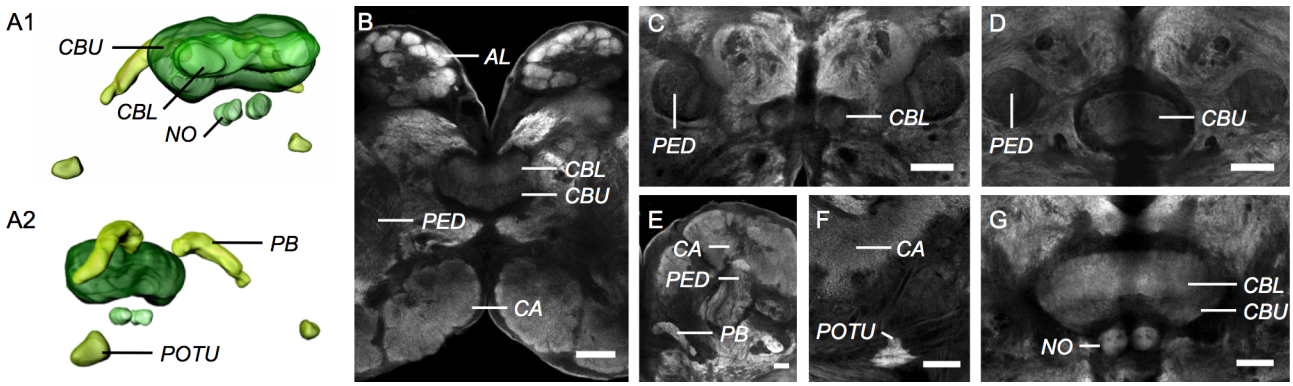
A1
CBU
CBL
NO
A2
PB
POTU
B
AL
CBL
CBU
PED
CA
C
PED
CBL
D
PED
CBU
E
CA
PED
PB
F
CA
POTU
G
CBL
CBU
NO

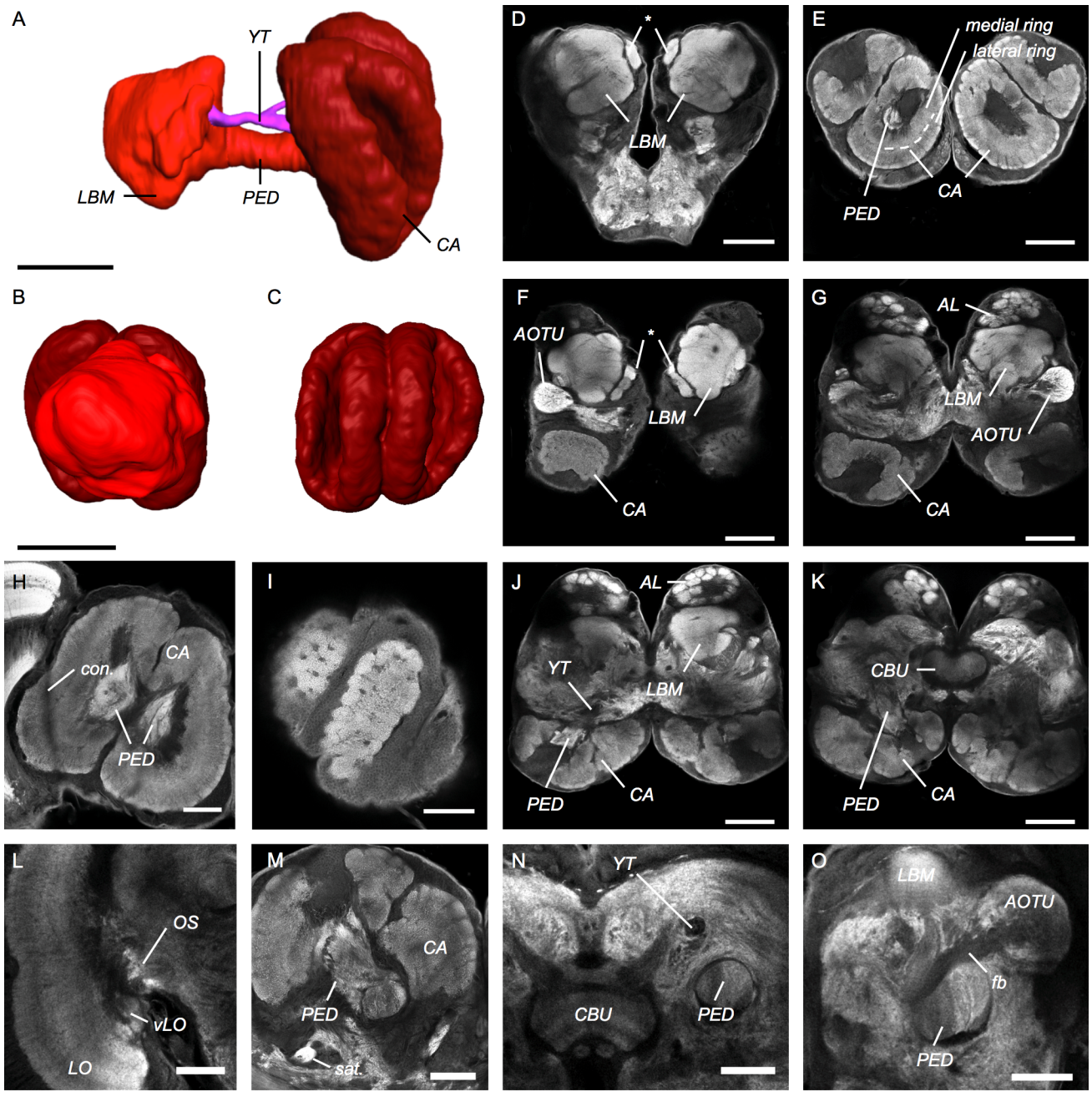
A
YT
LBM
PED
CA
B
C
D
*
LBM
E
medial ring
lateral ring
PED
CA
F
AOTU
*
LBM
CA
G
AL
LBM
AOTU
CA
H
con.
CA
PED
I
J
AL
YT
LBM
PED
CA
K
CBU
PED
CA
L
OS
vLO
LO
M
CA
PED
sat.
N
YT
CBU
PED
O
LBM
AOTU
fb
PED

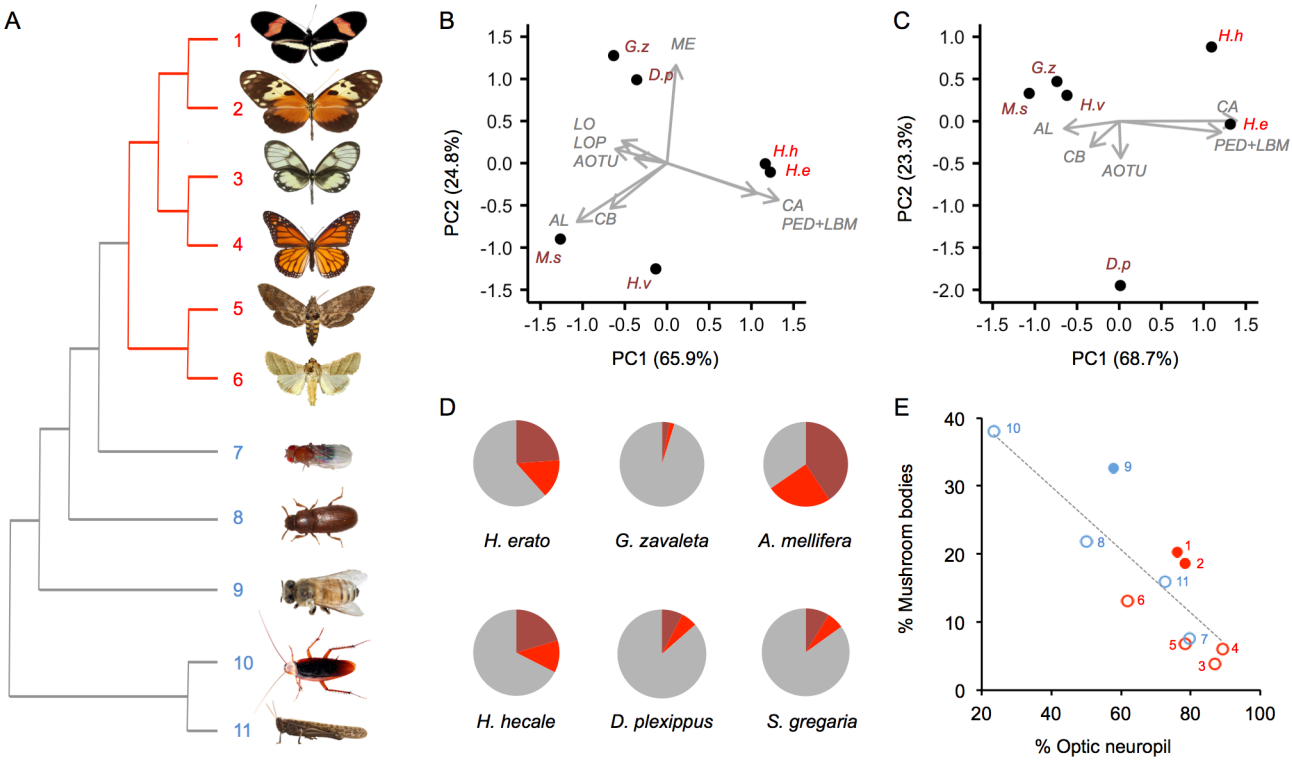
A
1
2
3
4
5
6
7
8
9
10
11
B
G.z
ME
D.p
LO
LOP
AOTU
H.h
H.e
CA
PED+LBM
AL
CB
M.s
H.v
PC2 (24.8%)
PC1 (65.9%)
C
H.h
G.z
M.s
H.v
AL
CA
H.e
PED+LBM
CB
AOTU
D.p
PC2 (23.3%)
PC1 (68.7%)
D
H. erato
G. zavaleta
A. mellifera
H. hecale
D. plexippus
S. gregaria
E
% Mushroom bodies
% Optic neuropil

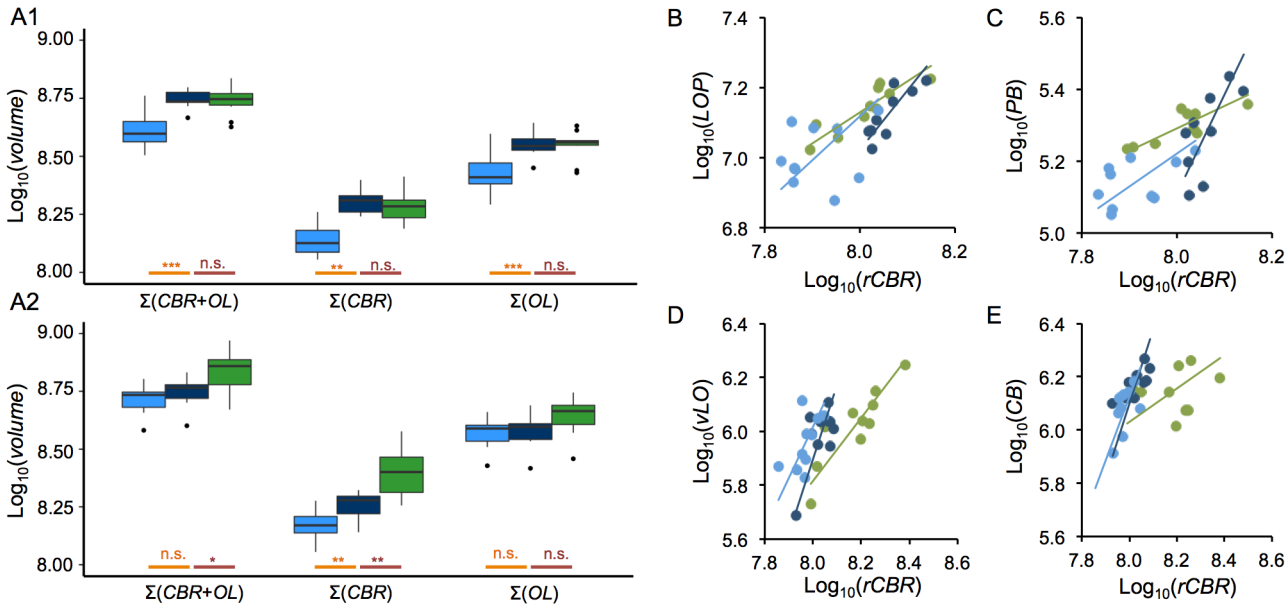
A1
A2
Log10(volume)
9.00
8.75
8.50
8.25
8.00
***
n.s.
**
n.s.
***
n.s.
Σ(CBR+OL)
Σ(CBR)
Σ(OL)
n.s.
*
**
**
n.s.
n.s.
B
C
D
E
Log10(LOP)
Log10(PB)
Log10(vLO)
Log10(CB)
Log10(rCBR)
7.4
7.2
7.0
6.8
5.6
5.4
5.2
5.0
6.4
6.2
6.0
5.8
7.8
8.0
8.2
8.4
8.6

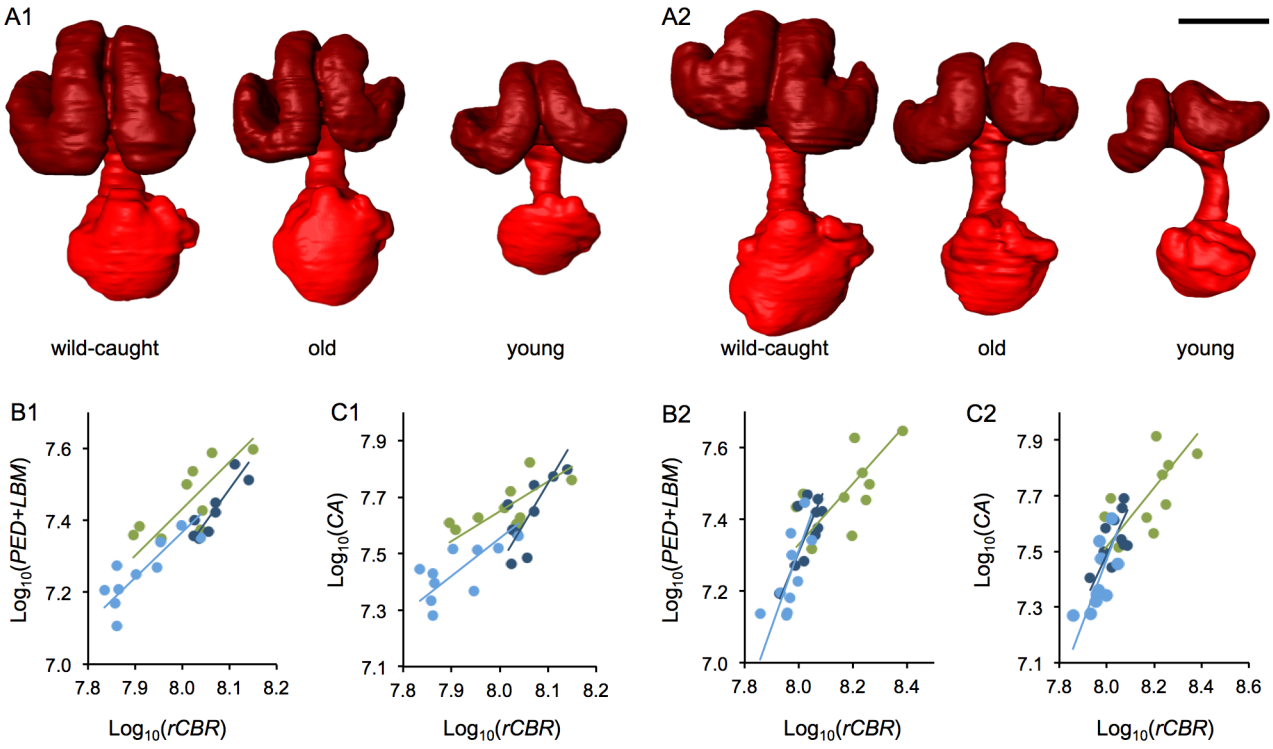
A1
A2
wild-caught
old
young
wild-caught
old
young
B1
C1
B2
C2
Log10(PED+LBM)
Log10(CA)
Log10(rCBR)
7.0
7.2
7.4
7.6
7.1
7.3
7.5
7.7
7.9
7.8
8.0
8.1
8.2
8.4
8.6